

Challenges in identifying Antarctic coastal polynyas in satellite observations and climate model output to support ecological climate change research

Laura Landrum¹, Alice K. DuVivier¹, Marika M. Holland¹, Kristen Krumhardt¹, Zephyr Sylvester²

¹NSF National Center for Atmospheric Research, Boulder, CO, USA

²INSTAAR, University of Colorado, Boulder, CO, USA

Correspondence to: Laura Landrum (landrum@ucar.edu)

Abstract. Antarctic coastal polynyas are key components of Antarctic marine ecosystems, influencing light and nutrient availability and open water access for marine predators. Thus, changes in the physical characteristics of polynyas can influence how these ecosystems respond to a changing climate. Here, we explore challenges inherent in identifying climatologically and biologically relevant Antarctic coastal polynyas on gridded data in both satellite and Earth System Model data. We find that it is critical to consider grid type and resolution, season, metric and threshold when defining polynyas. Regridding data, both spatially and temporally, can have significant impacts on identified polynya statistics. The spatial distributions of Antarctic coastal polynyas are significantly correlated between the two observational products between the observational products and the model data. The Earth System Model we use here captures coastal polynya-like features that occupy ~3% of the area of the winter sea ice zone and contribute ~17-21% of the total sea ice zone marine net primary productivity (NPP). Temporal auto- and cross correlations of integrated polynya areas and numbers are inconsistent across observational and modelling products. Trends in polynya areas are not robust, changing significance, magnitude and sign across threshold, grid and product.

1 Introduction

Polynyas, defined by the World Meteorological Organization as “any non-linear shaped opening enclosed in ice” and “may contain brash ice and/or be covered with new ice, nilas, or young ice” (WMO, 1970), can be found in the southern ocean both in open water and along the Antarctic coast. Open water polynyas are created when relatively warm ocean water upwells to the surface thermodynamically melting sea ice (“sensible heat polynyas”) – these are relatively uncommon and will not be discussed further in this work. Coastal polynyas are driven by cold downslope winds off the Antarctic continent that mechanically push sea ice away from the coast leaving open ocean water that can rapidly loses heat and freezes into more sea ice (“latent heat polynyas”). Many of coastal polynyas, particularly in Eastern Antarctic, are associated with land fast ice and grounded icebergs which influence the location and size of the polynyas formed through blocking ice advection (e.g. Fraser et al., 2019; Nihashi & Ohshima, 2015). Coastal polynyas occupy only a small area within the Southern Hemisphere sea ice zone yet play an outsized role in Antarctic sea ice production, deep water formation, global thermohaline circulation, carbon

Deleted: Defining

Deleted: Coastal

Deleted: Antarctic

Deleted: how to identify polynyas using

Deleted: ,

Deleted: and we assess the impacts of using different polynya-identification metrics and thresholds (sea ice concentration or thickness). Our results show optimal metrics for coastal polynya definition will depend on both the data resolution, as well as the season and region of interest. Temporal resolution (daily vs monthly) has an impact on polynya identification in specific regions and seasons and but has no significant impact on integrated hemispheric coastal polynya area. Our results highlight the importance of identifying polynyas on grids of the same type and resolution when comparing polynyas from different data products. We find that sea ice thickness is more suitable for identifying polynyas in model data in winter months in contrast to spring months when both sea ice thickness and concentration may be suitable metrics. The Community Earth System Model Version 2 (CESM2) identifies similar integrated Antarctic coastal polynya areas and locations as satellite based sea ice data, although polynyas identified in the CESM2 tend to be larger and fewer in number than those identified in the satellite products particularly in the winter. We then use the CESM2 to investigate ecosystem function within polynyas and find that there is enhanced phytoplankton productivity in modeled polynya features in both hindcast and fully coupled simulations. Springtime polynyas remain an important control on Antarctic productivity under future climate change, although the relative role of polynyas decreases as polynyas diminish and phytoplankton productivity outside of polynyas increases as sea ice cover decreases.

Deleted: are

Deleted: regions of reduced sea ice concentration surrounded by higher sea ice concentrations and/or coastline, and both

Deleted: (“sensible heat”) and

Deleted: coastal (“latent heat”) polynyas are found in the Antarctic sea ice zone

sequestration, and biological activity. Coastal polynyas produce about 10% of the total Antarctic sea ice (Tamura et al., 2008) and one polynya alone - the Cape Darnley polynya produces ~6-13% of the total Antarctic Bottom Water (Ohshima et al., 2013). As regions of lower sea ice concentration and/or thinner sea ice, polynyas are the first oceanic regions exposed to light in the Antarctic spring. As a result, polynyas show enhanced production within the Antarctic sea ice zone, where phytoplankton growth tends to be limited by light (Arrigo and van Dijken, 2003; Arrigo et al., 2015) and spring phytoplankton blooms within polynyas are frequently synchronized with light availability (e.g. Li et al., 2016). Polynyas also provide Antarctic predators (e.g., penguins, seals) both open water access and augmented prey resources, with ephemeral polynyas being of particular importance for Emperor penguins (Labrousse et al., 2019). Coastal polynyas are sometimes referred to both as “polynyas“ (indicating formation in the ice-growth season) and “post-polynyas“ (formation in the melt season by the rapid melting of the relatively thin sea ice), though in both cases they are recognized to impact in recognition of their important biological functions even when they may cease to be defined as “polynyas“ in the strict definition (e.g. Arrigo & van Dijken, 2003; Criscitiello et al., 2013).

How Antarctic marine ecosystems respond to a changing climate will be determined, at least in part, by changes in the sea icescape, including the size, location and timing of coastal polynyas. Antarctic polynyas are formed within the sea ice zone, and the sea ice around Antarctica has been studied extensively using both satellite and Earth system model (ESM) data. Satellite observations of sea ice (1979-present) show small positive trends in Antarctic sea ice area (the total area of sea-ice) and extent (defined as the area covered by sea ice concentrations of 15% or higher) until 2016 followed by unprecedented sea ice losses and changes in both persistence and variability (e.g., Fogt et al., 2023; Parkinson 2019; Purrich & Doddridge, 2023; Raphael & Handcock, 2022; Raphael et al., 2025; Turner et al., 2017; Turner et al., 2022). The most current ESMs contributing to the Climate Model Intercomparison Project phase 6 (CMIP6; Eyring et al., 2016) show a wide range of Antarctic sea ice states (e.g. Roach et al., 2020). Even though many ESMs capture the climatology of observed Antarctic sea ice, ESMs particularly struggle in particular to capture both the small, but significant, positive trend observed 1979-2015, and the more recent dramatic sea ice losses (Diamond et al., 2024; Roach et al., 2020). The recent, extreme losses and extended reconstructions of Antarctic sea ice suggest that there may be internal variability not captured by the relatively short observational record (e.g. Fogt et al., 2023; Hobbs et al., 2024; Holmes et al., 2024; and references therein). These assessments of Antarctic sea ice, however, focus predominantly on large-scale sea ice extent and area rather than the complex icescape within the ice pack where polynyas form.

Polynyas and polynya-like features often have scales and dimensions much smaller than those resolved by either satellite observations or global climate model data. For example, the median sizes of wintertime Antarctic coastal polynyas identified as key contributors to Antarctic primary production (e.g. Arrigo et al., 2016; Arrigo & van Dijken, 2003) and sea ice production (e.g. Tamura et al., 2008; Nihashi, S. & Ohshima, 2015; Tamura et al., 2016) range from 1.3 - 6 x10³ km², and many of these polynyas are relatively narrow (10-100km). Thus, many of these biophysically critical polynyas cannot be resolved on the

25x25 km grid of the passive microwave satellite data (e.g. Special Sensor Microwave Imager [SSM/I]), much less on the typically coarser $\sim 1^\circ$ ($\sim 100 \times 100$ km) resolution ESM grids. The challenge of identifying relatively smaller polynyas on relatively coarser grids has been explored in observational data products with a polynya signature simulation method (PSSM; Markus & Burns, 1995), which combines higher resolution 85Ghz frequency data with the high contrast data of the 37Ghz channel to classify SSM/I data as shelf ice, open water or sea ice (rather than SICs) and from which polynya maps can then be created at sub-pixel scales. This method has been applied to studies of marine productivity in Antarctic coastal polynyas (e.g. Arrigo & van Dijken, 2003; Arrigo et al., 2015). Tamura et al. (2006; 2007) address the resolution problem by combining SSM/I with the advanced very high resolution radiometer data (AVHRR) to estimate sub-grid scale sea ice thickness (SIT) in regions of thin sea ice. The resulting maps of sea ice thicknesses in thin sea ice areas along with reanalysis data from both the European Centre for Medium-Range Weather Forecasts (ERA-40) and the National Centers for Environmental Prediction (NCEP2) were used to make maps of sea ice production and variability in Antarctic polynyas (Tamura et al., 2007; Tamura et al., 2015). This method of identifying thin sea ice areas was applied in work investigating the influence of icescapes on Emperor penguin foraging habitat in East Antarctica (Labrousse et al., 2019).

The PSSM and sea ice production methods have been successfully used in identifying polynyas at sub-pixel scales in the satellite data, they are not directly applicable to ESM data which is saved as grid-cell averaged quantities. Polynya studies using ESMs thus use grid-cell averaged sea ice concentration (SIC) and/or thickness (SIT) thresholds to identify “polynya” grid cells of lower and/or thinner sea ice than the surrounding grid cells (e.g. Mohrman et al., 2021; DuVivier et al., 2024) – a method that has also been applied to satellite-based SICs (e.g. Massom et al., 1998; Duffy et al., 2024). These low sea ice grid cells are then labelled polynyas, although strictly speaking they identify grid cells that have a polynya-like feature within them per the given threshold rather than resolving individual polynya(s) within the grid cell. September Antarctic polynya areas in CMIP 6 models identified by SICs and SITs show particularly large inter-model spread in size and frequency across all CMIP6 models, and differences in coastal polynyas are attributed at least in part to differences in horizontal resolution although the impacts of different resolutions is not explored (Mohrman et al., 2021). ESMs compute sea ice production directly, which in turn can identify regions of high-sea ice productivity and thus infer coastal polynya regions – although resolution of these regions will still depend on the model grid (e.g. Joeng et al., 2023).

Satellite data and ESM output have different methodologies for determining SICs, which further complicate comparisons of polynyas and/or polynya-features identified in these products. Satellite SICs are retrieved from satellite microwave radiometers using sea ice algorithms which differ in their sensitivity to sea ice temperature and emissivity, atmospheric conditions (including winds, cloud liquid water vapor content, humidity), surface roughness in open water areas and the sea ice state and presence of liquid water on the sea ice (e.g. melt ponds). Uncertainties in satellite-based SICs tend to be greatest in summer season, and regions of low sea ice concentrations and thin ice (e.g. Meier, Windnagel and Stuart, 2021; Ivanova et al., 2015 and references therein). Earth system model SICs, on the other hand, are based on the physical evolution of simulated sea ice

135 due to fluxes of energy and momentum. ESMs calculate SICs to very small fractions/thicknesses (SITs), albeit with potential
biases from forcing or structural model uncertainty. Most ESMs use an ice thickness distribution (ITD) to represent the
heterogeneity of sea ice thicknesses within a grid cell. The average sea ice thickness of a grid cell is calculated as the total
volume of sea ice in the discrete thickness categories divided by the area of the grid cell. Satellite-derived SIT estimates are
becoming more readily available, however they remain spatially and temporally limited compared to SICs, particularly in the
140 Antarctic, and have considerable uncertainty compared with SIC products (e.g. Bocquet et al., 2024; Fons et al., 2022; Kacimi
& Kwok, 2022; Zygmuntowska et al., 2014 and references therein). Thus, SIT from satellite products has limited capacity for
identifying thin sea ice which may be relevant for polynyas, especially during the active ice-growth period of wintertime
coastal polynyas. Further, ESM SICs and SITs are calculated at the model time-step (e.g. every hour) then averaged over a
day for daily averages, whereas satellite microwave radiometer data represent an instantaneous snapshot of conditions specific
145 to a particular time and location (typically daily or bi-daily; Meier et al., 2014).

ESMs are powerful tools for exploring past, present and future climates and how polar marine ecosystems may respond to
climatic change, and satellite SIC data have been used extensively to validate sea ice areas and extents in ESMs. Earth system
models (ESMs) are increasingly being used to study polynyas in the climate system (e.g. Mohrmann et al., 2021; Jeong et al.,
150 2023; DuVivier et al., 2024) yet we are unaware of any publications that assess in detail how to best identify and compare
climatologically-relevant polynya-like features in both ESMs and satellite products. The following are the four primary
questions we address in this work:

1. Are coupled earth system models (ESMs) capable of capturing climatologically and biologically relevant coastal
polynya-like features?
- 155 2. How to best use observational products to validate coupled earth system model simulations of polynya-like
features?
3. Do these polynya-like features in ESMs occur in regions/areas where polynyas and polynya-like features are
identified in observations?
- 160 4. Do coastal polynya features in ESMs function in marine ecological processes as we believe they do in the real
world?

▼
We also seek to understand how choice of polynya metrics may influence results in terms of polynya area, location and trends
and location. We intend for this exploration to give guidance on implications of various polynya metric choices for model and
satellite-based data analysis. The role of low sea ice areas in Antarctic marine ecosystems is dynamic and diverse – polynyas
165 affect availability of light and nutrients for phytoplankton, provide open water access and thus prey for marine predators such
as penguins and seals, and the timing of low sea ice conditions influences the seasonal progression of phytoplankton blooms.
In this paper, we investigate the impacts of metric choices on coastal polynya identification, compare polynya areas estimated

Deleted: Defining polynyas as areas of relatively open water surrounded by sea ice and/or land, which is a common way to refer to these features, is a subjective definition which does not consider questions of scale and polynya functioning. In order to use climate models to investigate how Antarctic polynyas may change in the future, we need to both assess the impacts of different polynya definitions for gridded data and investigate how polynyas estimated from model output compare with those estimated from satellite images over the historical period. Objective and quantifiable methods to identify polynyas are necessary in order to assess their role in the climate and ecological system, compare observations with model output, and make inferences regarding future polynya change. Earth system models (ESMs) contributing to the Climate Model Intercomparison Project phase 6 (CMIP6) show a wide range of Antarctic sea ice states (e.g. Roach et al., 2020) and September polynya areas (Mohrmann et al., 2021). Open water polynyas show particularly large inter-model spread in size and frequency across all CMIP6 models, much of which may be due to differences in model hydrography and deep water convection, whereas differences in coastal polynyas is attributed at least in part to differences in horizontal resolutions and polynyas were identified across the models using the same thresholds regardless of grid resolution (Mohrmann et al., 2021). Biases in simulated Antarctic Sea ice will impact polynya identification as well – models that have very low mean sea ice states, for example, will consequently have a far smaller area over which it is possible for polynyas to form. ESMs struggle in particular to capture both small but significant positive observed trends in Antarctic Sea Ice, 1979-2015, and the more recent dramatic sea ice losses (Diamond et al., 2024; Roach et al., 2020). The recent, extreme losses and extended reconstructions of Antarctic sea ice suggest that there may be internal variability not captured by the relatively short observational record (e.g. Fogt et al., 2023; Hobbs et al., 2024; Holmes et al., 2024; and references therein).[†]

[†] Polynyas and polynya-like features often have scales and dimensions much smaller than those resolved by either satellite observations or global climate model data. Furthermore, sea ice concentrations (SICs) are calculated using different products and methodologies in observational data sets and climate model simulations. The long-term (since 1979) record of satellite SICs are retrieved from satellite microwave radiometers using sea ice algorithms. The retrieval algorithms differ in their sensitivity to sea ice temperature and emissivity, atmospheric conditions (including winds, cloud liquid water vapor content, humidity), surface roughness in open water areas and the sea ice state and presence of liquid water on the sea ice (e.g. melt ponds). Uncertainties in satellite-based SICs tend to (... [1])

Deleted: ive

Deleted: goals

Deleted: are to

Deleted: <#> explore different methods of defining polynyas based on gridded time series data, and to define metrics that are reproducible, verifiable, and useful for assessing polynyas in present and future climate states.[†] use these optimal polynya metrics to identify coastal polynyas in satellite based sea ice products and an atmospheric-reanalysis forced ocean-sea ice (FOSI) simulation for comparison of the regional and seasonal identification of coastal polynyas in both satellite and simulated sea ice products.[†] (... [2])

Deleted: frequency

from simulated and observed data, assess if our polynya metrics identify biologically important marine regions. This analysis provides comprehensive and quantifiable information on polynya identification that can be used in future work to assess the role of changing polynyas on Antarctic marine ecosystem dynamics and the physical environment.

Deleted: s, and apply these metrics to a large ensemble of historical and future climate scenarios

2 Data

2.1 Satellite observations

We consider two daily observational Climate Data Records (CDR) of gridded sea ice concentration data from satellite images: the [version 4 of the CDR of passive microwave SIC](#) developed at the National Snow & Ice Data Center (NSIDC) for the National Oceanic and Atmospheric Administration (NOAA; Meier et al., 2014; Meier et al., 2021) and the European Organisation for the Exploitation of Meteorological Satellites (EUMETSAT) Ocean and Sea Ice Satellite Application Facility (OSISAF) [SIC CDR \(OSI-450\) for 1979-2015 and the OSI-430-b from 2016-2020](#) (Lavergne et al., 2019). The NOAA data are a merged product of the NASA Team (Cavalieri et al., 1984) and Bootstrap (Comiso, 1986) algorithms, with the higher SIC of the two products used as the CDR value when the two products differ (Meier et al., 2014). Both the NOAA and OSISAF data are derived from the same satellite radiometer data using different sea ice retrieval algorithms. The largest differences in SICs resulting from different retrieval algorithms tend to be found in areas of relatively thin sea ice, where SIC tend to be underestimated across all algorithms (Ivanova et al., 2015; Kwok et al., 2007; Grenfell et al., 1992). We include the NOAA and OSISAF products of sea ice concentrations in this study to explore differences in identified polynya areas from observationally-based gridded SIC products that may result due to different sea ice retrieval algorithms. Both the NOAA and OSISAF CDRs are used extensively in the [ESM](#) research community [for model testing, validation and improvement](#).

Formatted: Font: Not Italic

Deleted: CDR

Deleted: CDR

Deleted: but by

Deleted: both

Deleted: The NASA Team product typically has the lowest SICs in areas of thin ice of the different retrieval methods, and although the NOAA CDR uses Bootstrap SICs where NASA Team SICs are lower, we show one example of polynyas identified using the NASA Team product for comparison. The remainder of our analysis uses the NOAA and OSISAF CDR for our observationally-based gridded sea ice products.

We calculate polynya maps for the NOAA and OSISAF products on both the original (25 km x 25 km) Equal Area Scaleable Earth (EASE) grid as well as regridded onto a nominal 1° climate model grid, as described below. The reason to create maps on both grids is to better understand the impact of resolution on the identification of polynyas across different products (i.e. satellite observations and Earth System Models) that span large spatial scales. Additionally, given the differences in instantaneous satellite observations and model average conditions, we apply our polynya metrics to daily and monthly averaged data to better understand the impacts of temporal resolution on polynya identification.

Deleted: climate model

Deleted: We use model output from two different configurations of the CESM2: an ocean-ice hindcast forced by atmospheric reanalysis data, and a fully-coupled configuration forced by the Coupled Model Intercomparison Project Phase 6 (CMIP6) protocols for the historical (1850-2014) and future (2015-2100) high emissions scenario (SSP370; Eyring et al., 2016). Both CESM2 configurations are on the standard nominal 1° grid.

Deleted: for

2.2 Climate Model Output

This study uses output from [a configuration of](#) the Community Earth System Model Version 2 (CESM2; Danabasoglu et al. 2020) for [representative ESM data](#). The JRA-CESM hindcast simulation (Krumhardt et al., 2024) is a prognostic ice-ocean simulation with CESM2 that is forced by the Japanese Reanalysis product (JRA-CESM; Kobayashi et al., 2015; Tsujino et al., 2018) [using reanalysis atmospheric conditions that match observed weather](#). [This hindcast simulation removes model-](#)

observational differences due to atmospheric forcing or internal variability and thus the simulated ice conditions and variability in the JRA-CESM are more directly comparable to the satellite products. Antarctic SICs and sea ice extents (SIE; defined as the area covered by sea ice concentrations of 15% or higher) in the JRA-CESM compare well, spatially and temporally (Krumhardt et al., 2024), with the NSIDC Climate Data Record (Meier et al., 2021) and the NSIDC Sea Ice Index (Fetterer et al., 2017).

The JRA-CESM is on a standard nominal 1° grid and uses the sea ice model (CICE) and Parallel Ocean Program (POP) ocean model. CICE is a thermodynamic-dynamic model that resolves subgrid-scale ice thickness distribution in five sea ice thickness categories. The CESM2 computes light penetration based on this subgrid-scale sea ice thickness, important for capturing the non-linear photosynthetic function in ice-covered waters (Long et al., 2015). CICE simulates thermodynamic (growth and melt rates of snow and ice from vertical conductive, radiative and turbulent heat fluxes) and dynamic (including advection and ridging) changes to sea ice concentrations and volume (Hunke et al., 2013). The CESM, like many ESMs, uses an Ice Thickness Distribution (ITD) scheme, with 5 thickness categories used in the JRA-CESM to parameterize sub-grid scale variations in ice thickness (e.g. Holland et al., 2006). Thermodynamics and dynamics operated on sea ice within each category. Grid cell averaged sea ice thickness is calculated by taking the sum of the volume of sea ice in each thickness category and dividing by the area of the grid cell. The sea ice component of the CESM2 includes a “mushy” thermodynamic component that allows for a mixture of brine and solid ice which leads to increases in both frazil ice production and Antarctic Bottom Water formation in polynya-like coastal features when compared with the earlier model version, the CESM1 (DuVivier et al., 2021; Singh et al., 2020). Coastal frazil ice production is particularly important in Antarctic coastal polynyas (e.g. Nakata et al., 2021 and references therein). The CESM2 hindcast simulations also use the Marine Biogeochemical Library (MARBL) model (Long et al., 2021), which simulates planktonic marine ecosystem dynamics and coupled cycles of carbon, nitrogen, phosphorus, iron, silica, and oxygen. MARBL is highly configurable, allowing a flexible number of plankton functional types – for this study MARBL is a slightly more complex ecosystem than in standard configuration, as described in Krumhardt et al. (2024). We focus on net primary productivity (NPP) here, which is the sum of net carbon fixation by all phytoplankton functional types. This paper presents a more in-depth view of polynya-like features in the CESM2 than previous related work (DuVivier et al., 2021).

3 Methods

3.1 Polynya algorithm

Our algorithm defines polynyas from a particular variable and threshold value. The two physical sea ice variables we focus on for polynya identification are SIC (observations and model) and SIT (model). Polynyas are identified as contiguous regions of grid cells that fall below a given threshold and are surrounded by land and/or ice-covered regions above the threshold (e.g. Appendix A). This method cannot resolve discrete polynyas on scales smaller than a grid cell, but rather identifies grid cells that contain fractions of open water (or thin sea ice) compared to surrounding grid cells. Model output is on a grid cell average

Deleted:

Deleted: The fully coupled simulations (Danabasoglu et al., 2020) use a standard configuration that was a contribution to CMIP6 (Eyring et al., 2016) and have fully prognostic atmosphere, ocean, sea ice, and land components. We utilize the CESM2 50-member Large Ensemble (CESM2-LE, forced with the standard CMIP6 forcing (CESM2-LE; Rodgers et al., 2021).

Deleted:

For ocean biogeochemistry, both CESM2 configurations were run with

Deleted: In this study, the fully coupled simulation uses the planktonic MARBL ecosystem described in Long et al (2021), while JRA-CESM uses a slightly more complex ecosystem,

Deleted: All configurations of CESM simulations compute light penetration based on a subgrid-scale sea ice thickness, important for capturing the non-linear photosynthetic function in ice-covered waters (Long et al., 2015).

The JRA-CESM hindcast simulation removes model-observational differences due to atmospheric forcing or internal variability. Thus, the simulated ice conditions and variability in the JRA-CESM are more directly comparable to the satellite products than the fully-coupled CESM and hence the bulk of our model-satellite polynya comparisons are based on this simulation. Antarctic SICs and sea ice extents (SIE; defined as the area covered by sea ice concentrations of 15% or higher) in the JRA-CESM compare well, spatially and temporally (Krumhardt et al., 2024), with the NSIDC Climate Data Record (Meier et al., 2021) and the NSIDC Sea Ice Index (Fetterer et al., 2017). The sea ice model (CICE) is a thermodynamic-dynamic model that resolves subgrid-scale ice thickness distribution in five sea ice thickness categories. CICE simulates thermodynamic (growth and melt rates of snow and ice from vertical conductive, radiative and turbulent heat fluxes) and dynamic (including advection and ridging) changes to sea ice concentrations and volume (Hunke et al., 2013). The sea ice component of the CESM2 used in all configurations shown here includes a “mushy” thermodynamic component that allows for a mixture of brine and solid ice which leads to increases in both frazil ice production and Antarctic Bottom Water formation in polynya-like coastal features when compared with the earlier model version, the CESM1 (DuVivier et al., 2021; Singh et al., 2020). Coastal frazil ice production is particularly important in Antarctic coastal polynyas (e.g. Nakata et al., 2021 and references therein).

Deleted: polynyas

and does not contain information regarding the distribution of open water within the grid cell such as leads, polynyas, regions of new ice etc., and thus these areas are more accurately described as “polynya-like features” although we will continue to use the term “polynya” for brevity. The first step in the algorithm identifies all grid cells that fall below the variable threshold and lie within the ice zone (i.e. not immediately bordering open ocean). In subsequent iterations, the algorithm checks neighbouring grid cells. If all grid cells bordering a region of ice below the threshold are bounded by higher threshold variables and/or land, then this region is identified as a polynya (or polynya-like feature, as noted above). If any neighbouring cells are bounded by open ocean, the grid cells are not considered a polynya even though they meet the threshold requirement. This iterative process is necessary in some regions and seasons when the northern ice edge may be complicated as polynyas open up and merge with open water (e.g. in the Ross Sea in austral spring and around the Western Antarctic Peninsula with a relatively complicated coastline). The polynya algorithm also numbers individual polynyas and calculates polynya areas based on the number of grid cells each individual polynya occupies. In this manner, we can calculate not only total polynya area by region, but also the number of individual polynyas and their sizes. This threshold-based algorithm is similar to the method employed by Mohrmann et al. (2023), and we identify polynyas for a range of threshold values for satellite-based SICs and model-based SICs and SITs. Our algorithm maps both open-water (surrounded by higher concentrations or thicknesses of sea ice) and coastal (at least one grid-cell neighbouring land) polynyas, but this work focuses primarily on coastal polynyas because of their important ecological functions and because open ocean polynyas are relatively uncommon in observations and in the model results.

Deleted: but

We first explore the influence of polynya metrics on polynya identification in the satellite and JRA-CESM data by calculating integrated total “polynya areas” (the area of grid cells containing polynya-like features) by different time periods (seasonal, annual, monthly) and region (Southern Hemisphere and smaller regions using the regional definitions of Parkinson & Cavalieri, 2012 and shown in Fig. 1f) for winter (June-July-August; JJA) and spring (September-October-November; SON). We focus on winter-spring as these seasons are key for formation of coastal polynyas as well as light and nutrient availability for marine productivity. We then choose one SIC and one SIT polynya threshold metric to apply to the satellite products and the JRA-CESM to explore spatial and temporal relationships between these different products at a given threshold. The thresholds chosen are based on results from the range of possible thresholds and represent a compromise with regards to number of polynyas and total integrated southern hemisphere (SH) polynya area. We aim for a total number of polynyas within the observational range, winter-spring, for sea ice production (13; Nihashi & Ohshima, 2015; Tamura et al., 2008) and high marine productivity (37-46; Arrigo & van Dijken, 2004; Arrigo et al., 2015). The total area of polynyas in our method represents the area of grid cells labelled as containing polynya-like features, and therefore we pick thresholds that lead to polynya-gridcell-areas at least as large if not larger than the lower ranges of published observational estimates for these seasons ($\sim 1 \times 10^6 \text{ km}^2$; e.g. Arrigo & van Dijken, 2004; Arrigo & van Dijken, 2004; Tamura et al., 2008; Nihashi & Ohshima, 2015).

Deleted: 50-member CESM2-LE.

Deleted: are based on the analysis of the integrated polynya areas from the satellite products and the JRA-CESM simulation compared with published estimates of Antarctic coastal polynya areas.

3.2 Impacts of metric thresholds, spatial and temporal resolutions on polynya identification

485 We apply a range of SIC (15%-85%) and SIT (10-85 cm) thresholds to identify polynyas in the two satellite products (“OBS”) and the JRA-CESM on different spatial and temporal resolutions. Polynyas often have scales and dimensions much smaller than that resolved by standard gridded sea ice data, even the relatively fine resolution OBS data on a 25km² EASE grid. Thus, appropriate threshold values for identifying polynyas may depend on the size of the data grid cell. As a simplified example, a polynya defined by a 10% SIC threshold on a 6.25 km EASE grid (e.g. the sub-pixel grid used by Arrigo & VanDijken, 2003) and surrounded by grid cells of 100% SIC would be classified as a polynya on 25/45 km EASE grids at 94/98% SIC thresholds (e.g. Appendix B). Polynya threshold choices are further complicated by climate model grids that tend to be in degrees latitude/longitude rather than equal-area grids. A given SIC threshold for the equal area grid is the equivalent of an area threshold (i.e. km² of open water within a grid cell), whereas on the equal-latitude/longitude grid a given SIC will correspond to different total open water areas within a grid cell depending on latitude (since the grid cell surface area is latitude-dependent, and thus a percentage of the total grid cell area will represent a different area depending on latitude; see Appendix B). Given these considerations and the scientific question at hand, the threshold used may need to depend on grid size and may be specific to region, season, and variable. We explore the impacts of grid size on polynya areas by making polynya maps from different grid sizes in the satellite data – the original 25 km EASE grid and regridded to the standard nominal 1° CESM grid. We compare polynya metrics between satellite and climate model output by focusing on the regridded satellite data.

500 Polynya-like features can change rapidly in time, particularly for wintertime Antarctic coastal polynyas when surface air temperatures are extremely cold and extensive (albeit thin) sea ice can form rapidly at open water surfaces. Polynyas identified from daily data, for example, may not appear on monthly time scales (particularly in the model, which can simulate high concentrations of very thin sea ice). We investigate the effects of temporal resolution on polynya identification by comparing polynyas estimated from daily and monthly data in both the satellite product and the model output.

3.3 Impacts of differing methodologies for calculating sea ice concentrations in the model and satellite images

Comparing polynya estimates in models and satellite observations is not a trivial matter. ~~Uncertainties increase in the passive microwave retrievals of SIC where concentrations at low concentrations ~10%. As a result, the National Snow & Ice Data Center (NSIDC) Climate Data Record (CDR) implements a 10% minimum threshold on the CDR data product (Meier, Windnagel and Stuart, 2021). Satellite-based SICs are underrepresented in areas of thin sea ice across all retrieval algorithms, particularly where sea ice thicknesses are below 25 cm (Ivanova et al., 2015). Sea ice between 5 and 20 cm thick will result in systematically underestimated SICs (Ivanova et al., 2015). In contrast, climate model simulations calculate SICs to very small fractions independent of mean SIT. This complicates how a polynya is identified in each dataset. For example, winter-time polynyas can be regions of extremely high sea ice production where sea ice forms nearly as fast as winds expose water to the overlying atmosphere. In these conditions, one might expect polynya metrics based on SIT would be more appropriate than~~

Deleted: Passive

Deleted: algorithms struggle to detect

Deleted: sea ice when

Deleted: fall below

520 SIC in model output as the extreme cold wintertime air temperatures can lead to nearly immediate sea ice formation and thus high SICs even if SITs are very thin. Conversely, SICs are underestimated in satellite products when the ice is very thin, so a satellite observation in these conditions should show lower SIC (note that observations of SIT are very limited). This is a clear example where SICs may be better suited for defining wintertime polynyas from satellite images whereas SITs might be a better metric from climate model output.

525

Given the challenges of passive microwave measurements and retrieval algorithms to estimate sea ice [concentrations](#) in low concentration and thickness conditions, as detailed above, we explore the influence of different definitions for SIC in satellite-based observations and model output by degrading the JRA-CESM hindcast sea ice concentrations such that the modified SICs are more closely aligned with SICs as they would be remotely sensed. Model SICs are degraded by setting daily SIC in grid cells with less than 10% SIC or less than 5 cm daily SIT to 0% SIC, closer to the values that a satellite would observe in these conditions. Daily SICs within grid cells that have SITs of 5-20 cm thick are set to half of the original model SIC output, [corresponding](#) to the underestimation of ice concentration over thin ice by satellites (Appendix C). Although using daily averaged data is not the same as the instantaneous satellite-snapshot data, it is the highest frequency model output of sea ice data available. We compare the degraded model SIC to the original output to gain insight into how differences in SIC methodologies may impact polynya identification in both observed and model data products.

535

3.4 Influence of metrics and resolutions on polynya identification

One of our primary goals in this work is to better understand how different metric choices on a variety of gridded data products will influence polynya identification, and how to best compare polynyas identified in both observational and simulated data [for model validation purposes](#). We explore both the influence of resolutions (temporal and spatial grid size) and metric thresholds. We identify polynyas over a range of SIC thresholds (15%-85%) throughout the year in the satellite based observations on the original EASE grid, regridded to the nominal 1° model grid, and [for](#) both daily and monthly-averaged data. Similarly, we apply the same range of SIC thresholds as well as a range of SIT thresholds (10-85 cm) to the daily and monthly JRA-CESM. We analyze these results [for winter and spring](#), and on regional and hemispheric scales to elucidate how the influence of polynya identification metric choice may differ by [season](#) and region. Based on the analysis of the NOAA and OSISAF CDRs and JRA-CESM, we pick two polynya identification metrics (85% SIC and 0.4 cm SIT thresholds on monthly averaged sea ice data) to [further explore similarities and differences in resultant temporal and spatial polynya area time series of the two satellite-based data products and the JRA-CESM to highlight impacts of temporal and spatial regridding, different observational data product choices, and model-observational comparison.](#)

545

3.5 NPP and polynyas

550 Polynyas play important roles in physical and biological processes, and optimal metrics for defining polynyas may differ depending on analytical goals. Here we explore what constitutes an optimal model-derived polynya metric based on their

Deleted: which

Deleted: by month

Deleted: time of year

Deleted: apply to the 50-member CESM2 over the historical (1850-2014) and future scenario (2015-2100) time periods. These polynya time series serve as the basis for our exploration of changes in both polynyas and NPP within polynyas in the future climate.

ecosystem-relevance, specifically their relation to NPP. During the austral spring (September-October-November), sea ice is melting and directly impacting NPP through light availability. During this season the optimal choice of metric (SIT or SIC) to define polynyas is not clear, and as such we pick one metric based on SIC and another on SIT to identify polynyas and investigate if these springtime polynya areas have increased productivity in the JRA-CESM model simulations by calculating NPP both within the polynya areas and within the sea ice zone (SIZ) as a whole. The SIZ is defined as the region south of the mean wintertime (June-July-August) northern pack ice (SIC $\geq 85\%$) boundary. Thus, regions within the ice pack and near the coast that may have lower sea ice concentrations or ice thicknesses (i.e. “polynyas”) lie within the SIZ. The goal is to help inform choices in future studies particularly when using model output that may not include marine biology components or that do not allow for trophic transfers to higher trophic levels as is critical for high latitude, light-limited systems.

4 Results

4.1 Large-scale sea ice properties

The CESM2 captures observed Southern Hemisphere (SH) sea ice area means as well as temporal and spatial variability quite well compared to CMIP6 models (e.g. Roach et al., 2020), and simulates coastal polynya-like features of high sea ice production (Singh et al., 2020; DuVivier et al. 2021). The CESM2 hindcast, forced by atmospheric reanalysis, underestimates total SH sea ice areas (SIA) from July through October by $\sim 10\text{-}14\%$ ($\sim 1.4\text{-}2.6 \times 10^6 \text{ km}^2$) compared with both the NOAA and OSISAF products (Fig. 1e; NOAA and OSISAF sea ice areas are very slightly different – Supplemental Figure 2 – so only the NOAA CDR is shown here). Regionally, both the JRA-CESM tends to underestimate Antarctic sea ice in the Weddell Sea for all months of the year and in the Indian sector in the winter through spring months (Fig. 1 and Supplemental Fig. 1).

Deleted: e.g

Deleted: 3.6 Polynyas and NPP in a changing climate

In this section we explore how both polynyas and NPP change from the historical time period into the future under the SSP3-7.0 emissions scenario. We compare results from the CESM2-LE during the historical period with results from the JRA-CESM and the CDR satellite records for context. We calculate integrated hemispheric NPP both within the SIZ and within springtime polynyas in the CESM2-LE, comparing both timeseries throughout the historical and future scenarios, and the climate mean annual cycle of NPP at the beginning (2001-2020) and end (2081-2100) of the 21st Century. We leave analysis of how future changes in NPP may be related to changes in trophic transfer and phytoplankton function types to future work.

Deleted: JRA-

Deleted: and the CESM2-LE generally

Deleted: Both versions of the model

Deleted: used for this study

Deleted: ocean-ice and fully coupled model simulations

Deleted: The largest differences between the JRA-CESM and fully coupled CESM2-LE datasets are found in the Weddell sea and Indian sectors. During the austral summer in the Weddell Sea, the CESM2-LE has substantially more sea ice than the JRA-CESM although still less than the satellite products. From winter through spring, the CESM2-LE underestimates sea ice in the Indian sector compared with both OBS, however the JRA-CESM simulates more sea ice in this region than the CESM2-LE particularly during the winter. The CESM2 simulations represent a reasonable selection of climate model for identifying Antarctic polynyas because both JRA-CESM and CESM2-LE fully coupled configurations capture the mean climatology of Antarctic sea ice, particularly compared with CMIP6 models (Roach et al., 2020) and simulate coastal polynya-like features of high sea ice production (Singh et al., 2020; DuVivier et al. 2021).

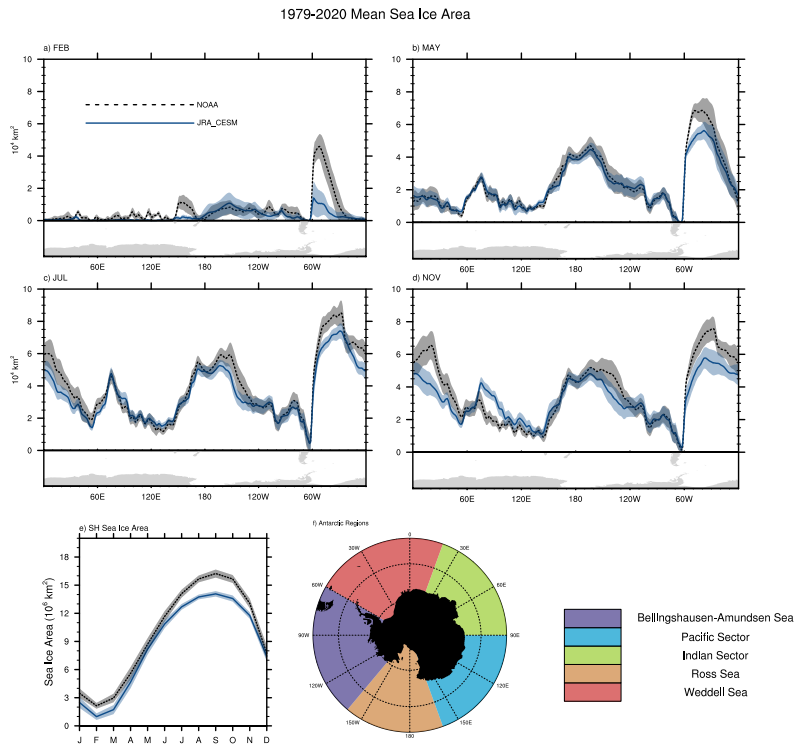
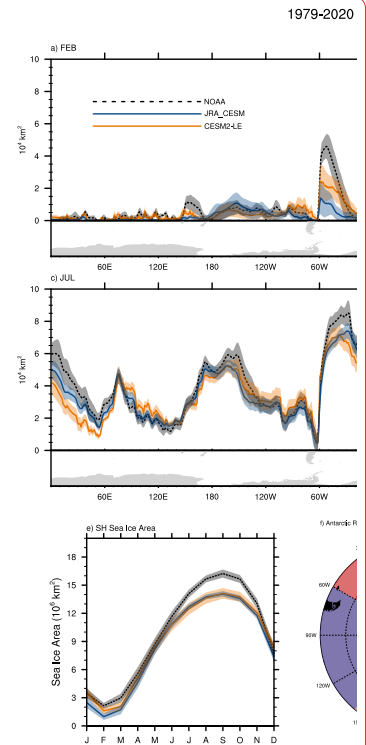


Figure 1. 1979-2020 Monthly mean total sea ice area as a function of longitude for a) February, b) May, c) July, d) November, e) monthly Southern Hemisphere (SH) sea ice area climatology for the NOAA CDR (black) and JRA-CESM (blue); and f) Antarctic regions map. Thick dashed (NOAA) and solid (JRA-CESM) lines indicate the mean, shaded polygons indicate the mean ± 1 standard deviation. Sea ice areas as a function of longitude have been smoothed by a 3-point running average.

4.2 Polynyas in the satellite data

Maps of open water and coastal polynyas on July 15, 2003, calculated using our algorithm and a SIC threshold of 85% for observational datasets are shown in Fig. 2 (a-e). Note that this date is not special, but a representative day shown to illustrate differences in polynya identification metrics across products. We picked a random winter day as relatively few polynyas are identified in January-April in all data products, and the broad similarities and differences between polynyas identified in different data products on this winter day are typical.



Deleted:

Deleted:),

Deleted: and CSM2-LE (orange) data

Deleted: , CSM2-LE

Deleted: (or ensemble mean for the CSM2-LE)

Deleted: (Supplemental Figs. 2-3)

Deleted: polynya area variabilities increase substantially for all metrics in November-December,

615

620

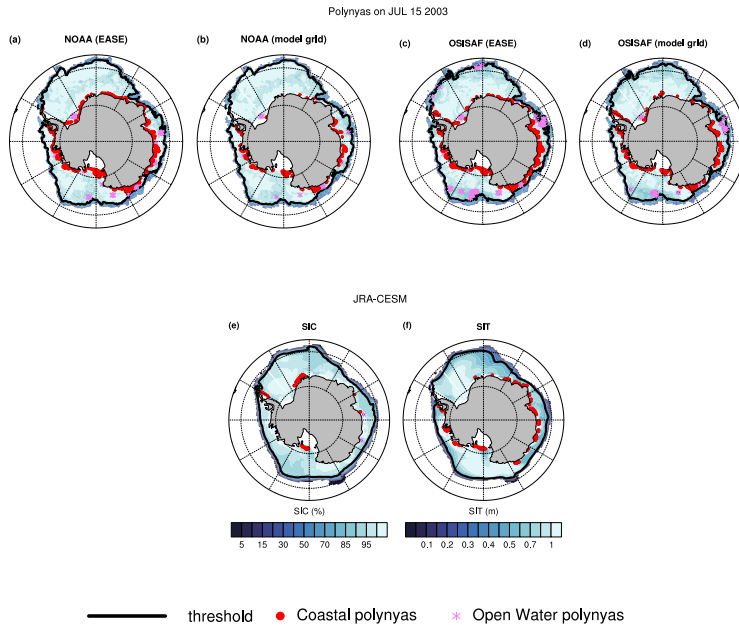
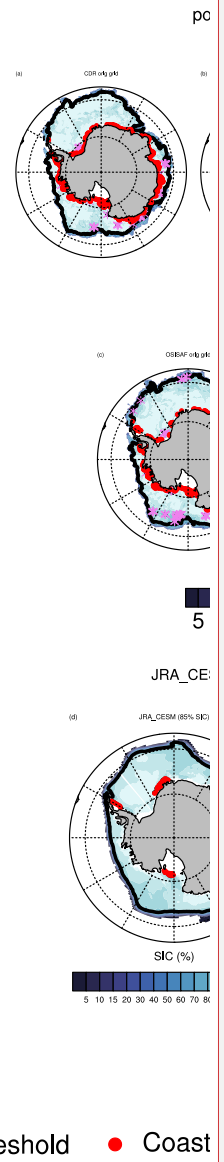


Figure 2. Polynya maps for July 16, 2003 using SIC 85% threshold for the NOAA and OSISAF CDR data on the original Equal Area Scaleable Earth (EASE) grid (a, c), the NOAA and OSISAF data regridded to the CESM grid (b, d), the JRA-CESM (e) and the JRA-CESM using a 0.4m SIT threshold (f). Open water and coastal polynyas are indicated by the pink stars and red dots. The 85% SIC and 0.4m contours are indicated by the thick black contours over the colour-contoured SIC or SIT values. Sea ice concentrations below 15% are masked out.

The sea ice edge (defined as the 15% SIC contour) is nearly identical for both the NOAA and OSISAF satellite products on the original grid and after regridding to the nominal 1° climate model grid (Fig. 2a-d). More open water polynyas are identified in the OSISAF product than the NOAA. Differences in coastal polynyas identified in the two satellite products are more mixed, with more coastal polynyas identified on the east side of the Antarctic peninsula in the OSISAF CDR than in the NOAA CDR, regridded or not, yet more coastal polynyas in the Weddell Sea in the NOAA product on the EASE grid than in the OSISAF. Regridding has a greater impact on polynya areas in the NOAA product than on the OSISAF product (Fig. 2 a-e and Fig 3 a-d). We show both open water and coastal polynyas identified in our example day, however we focus on coastal polynyas for the remainder of this study.



Deleted: Deleted: and ...or the NOAA and OSISAF CDR data on the original Equal Area Scaleable Earth (EASE) grid (a, d...), the OBS ...OAA and OSISAF data regridded to the CESM grid (b, e...), the NASA Team SIC product regridded to the CESM grid (c), and...the JRA-CESM (f...) and the JRA-CESM using a 0.4m SIT threshold (g) ... [3]

Deleted: all ...oth the NOAA and OSISAF satellite products – NOAA and OSISAF CDRs ...n the original grid, ...and after regridded ...egridding to the nominal 1° climate model grid, and the NASA Team satellite product - even though the edge of the pack ice (defined as 85% or higher SIC) is much further away from the sea ice edge in the NASA Team product ...Fig. 2a-e...). More open polynyas are identified in the OSISAF product than the NOAA. Differences in coastal polynyas identified in the two satellite products are more mixed, with more coastal polynyas identified on the east side of the Antarctic peninsula in the OSISAF CDR than in the NOAA CDR, regridded or not, yet more coastal polynyas in the Weddell Sea in the NOAA product on the EASE grid than in the OSISAF. Regridding has a greater impact on polynya areas in the

770 **4.2.1 Southern Hemisphere polynya statistics in satellite based products**

When moving beyond an example day and looking across all years, regridding the NOAA data from the original EASE grid to the model grid has a larger impact on both number and area of polynyas identified than for the OSISAF product (Figure 3a-d). The climatological winter and spring polynya areas and number of polynyas at a given SIC threshold in both observational products show only small changes when using monthly vs daily data (after regridding to the model grid). Integrated southern hemisphere (SH) coastal polynya areas as well as number of polynyas are larger in the NOAA product when identified on the original finer-resolution EASE grid than when regridded to the 1° CESM grid in both winter and spring across the full range of SIC thresholds. Polynya areas in the regridded NOAA product are nearly the same using both daily and monthly averaged data. On the other hand, regridding the OSISAF data to the model grid leads to larger polynya areas and higher numbers at SIC thresholds below ~70%, with smaller differences (within the 1 standard deviation range of polynyas identified on the EASE grid at daily resolution) higher thresholds. Like in the NOAA data, the differences in the climatological polynya areas and numbers between regridded daily and monthly data are quite small (Figure 3 a-d; see Supplemental Figure 3 for summer, DJF, and fall, MAM). Although integrated SH polynya areas are nearly identical across a range of thresholds from both satellite products on the original EASE, daily grid, regridding has opposing impacts on polynya identification in the two satellite products. After regridding to the model grid, consistently higher polynya areas and numbers are identified in the OSISAF data than from the NOAA data for both season and across the entire range of thresholds. Variability in SH polynya areas tends to be larger during the spring, particularly at high SIC thresholds, and continue to increase into the summer as areas of low/thin sea ice within the icepack merge with surrounding open ocean as the sea ice melts and contracts.

Deleted: Integrated

Deleted: areas, numbers and

Deleted: sizes

Deleted: data

Deleted: the primary differences in integrated total SH area of coastal polynyas in the NOAA CDR as identified by SIC threshold values arise from grid resolution during the late fall through early spring (May-October; Fig. 3 a-b and Supplemental Fig. S3)

Deleted: for a given threshold

Deleted: high

Deleted: from April through October

Deleted: the regridded

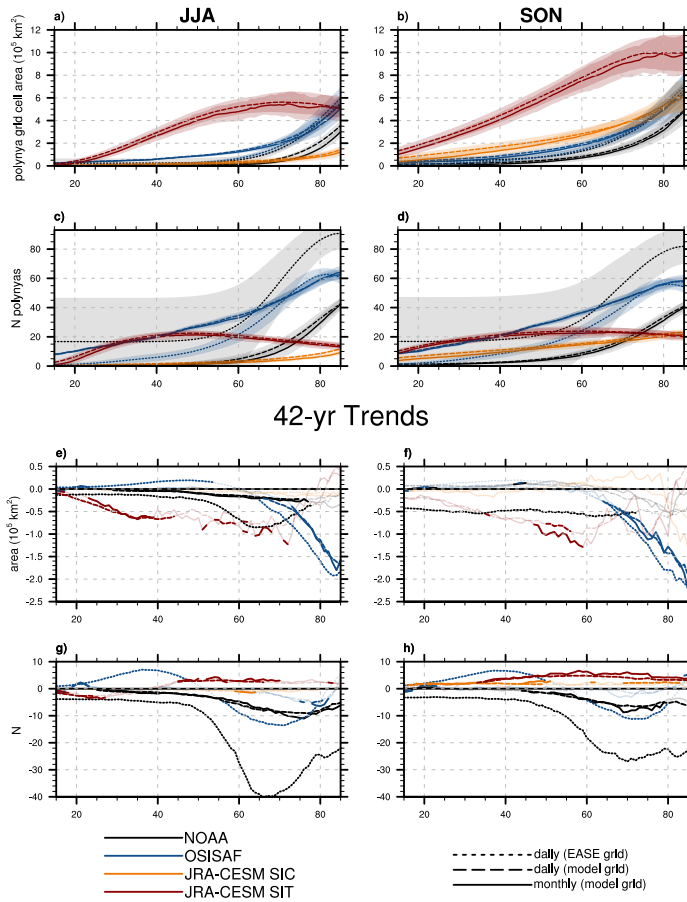
Deleted: either spatially or temporally has little effect on integrated SH polynya areas identified in the OSISAF CDR

Deleted: and Supplemental Figure S4

Deleted: ice retreat season November-January)

Deleted: in both CDRs (Fig. 3b, d and Supplemental Figs. 3-4). Throughout most of the year, differences due to temporal resolution are much quite small at a given threshold. More grid cells are identified as polynyas in the NOAA CDR, and the total SH polynya area is larger on the original, smaller resolution EASE grid than on the regridded data for a given threshold value. A given SIC threshold in the monthly regridded data identifies a larger SH polynya area in the OSISAF CDR than in the NOAA CDR.

SH coastal polynyas (1979-2020)



815 **Figure 3.** Total SH mean (1979-2020) coastal polynya areas (a-b), number of polynyas (c-d), 42-yr trends in polynya areas (e-f) and 42-yr trends in number of polynyas (g-h) as a function of threshold value (SIC, SIT) for winter (JJA; left column) and Spring (SON; right column) for NOAA (black), OSISAF (blue), and JRA-CESM (SIC metric, orange and SIT metric, maroon). Polynyas identified using the daily observational data on the original EASE grid are shown by dotted lines; dashed/solid lines indicate polynyas identified using daily/monthly data on the model grid. Climatological mean (1979-2020) values are shown in the thick lines; ± 1 standard

820 deviations shown by the lighter shading (a-d). Dark, thick dots/dashes/lines in the trends figures (e-h) indicate 95% or higher significance based on the Mann-Kendall non-parametric trend significance (Mann 1945; Kendall 1975; Gilbert 1987).

825 Trends in polynyas identified in the observational products differ by retrieval method, SIC threshold and spatial and temporal grids. Significant negative trends (and no significant positive trends) are seen for the NOAA daily CDR on the EASE grid in both seasons across all SIC thresholds for the number of polynyas, and at SIC thresholds less than ~76%/72% for the JJA/SON integrated polynya areas. On the other hand, polynyas identified in the OSISAF product show significant positive trends in area (JJA) and number (JJA, SON) at low SIC thresholds, and significant negative trends at high SIC thresholds (SH polynya areas and numbers, both seasons). After regridding to the model grid, integrated SH polynya trends are negative and significant only in the winter and at SIC thresholds lower than ~75% in the NOAA product and significantly smaller in magnitude (up to ~3-fold), and yet negative in both seasons in the OSISAF product and at SIC thresholds higher than ~65%. These

830 inconsistencies in trends across thresholds, observational data products and grids is also apparent in the regionally integrated timeseries with the exception of the Bellingshausen-Amundsen sea region which shows significant negative trends in polynya areas for both CDRs, on both the EASE and model grid, across a range of thresholds for the winter season (Supplemental Figures 4-8).

835 To better illustrate and compare relationships between polynya areas, numbers and locations, we show in more detail polynyas identified in observational and model data at select SIC and SIT (model) thresholds. We pick threshold values such that the resultant seasonal coastal polynya areas and numbers are consistent with published work (e.g. Arrigo & Van Dijken, 2003; Arrigo et al., 2015; Tamura et al., 2008; Nihashi & Ohshima, 2015), as outlined in our methods section, and such that integrated SH polynya areas are roughly equal in both seasons between all data sources and grids. We recognize that there is not one

840 clear choice of metrics and therefore our thresholds are somewhat arbitrary. Alternative threshold choices we have tried do not change our results (not shown). The metrics and thresholds we use for the satellite products are SIC threshold values of 78% and 85% for the EASE daily, and 85% for the regridded NOAA (daily and monthly) data, and 75% for the OSISAF (all grids).

845 Although in general the integrated SH polynya areas are very similar between these metric choices in these data products, there are some small differences in areas, numbers of polynyas, and variabilities (Figures 3a-d, 4). Notably, a larger number of distinct polynyas are consistently identified in the OSISAF data than in the NOAA data (regridded to the 1° grid and monthly averaged), and thus even though the SH polynya areas are quite similar, the average polynya size in the OSISAF is smaller than in the NOAA product.

Deleted: means, variability, trends, seasonalities and regionalities across the OBS and the climate model

Deleted: use

Deleted: metrics and thresholds that result in total 1979-2020 climatological SH polynya areas similar to those estimated from observations in other studies (e.g. Arrigo & Van Dijken, 2003; Tamura et al., 2008; Nihashi & Ohshima, 2015).

Deleted: and

Deleted: , monthly

Deleted: CDR

Deleted: CDR

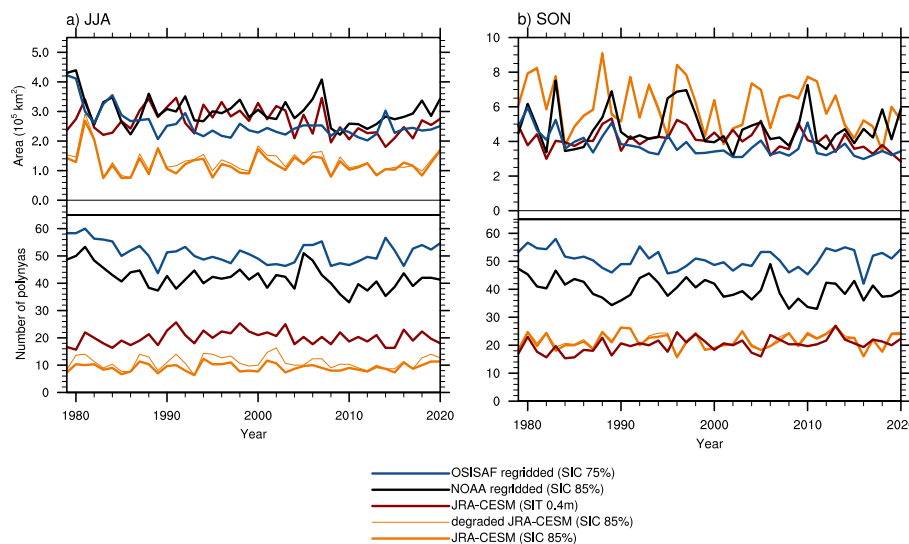
Deleted: Table 1,

Deleted: and Supplemental Figures 3-4, Supplemental Figure 6

Deleted: (Table 1)

Deleted: The number of polynyas identified in the OBS on the EASE grid is roughly twice as large as the number identified on the 1° model grid (Table 1), underscoring a possible complication when comparing polynyas estimated from different grid sizes (e.g. Appendix B). Additionally, variability in November SH polynya areas is more than double in the NOAA CDR than in the OSISAF CDR. Trends in wintertime (July) SH polynya areas are significant and negative across the satellite products, however the November trends are not significant in the NOAA regridded monthly data, whereas they are negative and significant in the OSISAF data and the NOAA data on the original EASE grid.

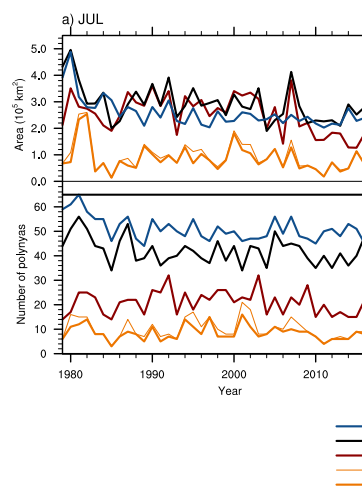
SH coastal polynyas 1979-2020



875 **Figure 4. Southern Hemisphere (SH) 1979-2020 winter (JJA: a) and spring (SON: b) mean coastal polynya area (top panels) and number of individual polynyas (bottom panels). Polynya timeseries are for monthly NOAA (SIC 85%; black) and OSISAF (SIC 75%; blue) CDR data regridded onto the CESM grid, JRA-CESM model simulation using monthly SIC (85%; orange) and SIT (0.4m; brown), and the JRA-CESM model SIC degraded to more closely mimic satellite SICs (85%; orange thin line).**

880 **Correlation coefficients reveal impacts of regridding (spatially and temporally) as well as relationships between the two observational products** (Figure 5). **Regridding then monthly averaging the SICs before identifying polynyas results in a significant loss of autocorrelation within the NOAA product particularly for integrated SH polynya areas. Timeseries of SH polynya areas from the daily data on the EASE grid and from the regridded, monthly averaged grid are not significantly autocorrelated for either season for the NOAA data product. Cross correlations for polynyas identified from the two observational products are significant only for polynyas identified from daily data (EASE and model grids), however the SH polynya timeseries (both areas and numbers) are not significantly cross-correlated between the observational products after regridding and monthly averaging. Auto- and cross correlations are comparable for the number of polynyas identified from the daily data (Figure 5b). Additionally, the cross-correlation coefficients between the daily observational products, although**

SH coastal



Deleted:

Deleted: 1979-2020 SH coastal polynya mean area, mean number, and trends [5]

Formatted: Font: 10 pt

Deleted: Table 1. Climatological Southern Hemisphere (SH) polynya area mean (and standard deviation), number of polynyas mean (and standard deviation), average polynya size and Theil-Sen non-parametric linear trend in total polynya area and number of polynyas for polynyas identified on the CESM nominal 1° grid and monthly data except where otherwise specified. Bold text indicates trends that are at 95% or higher significance based on the Mann-Kendall non-parametric trend significance (Mann 1945; Kendall 1975; Gilbert 1987).

We also calculated correlations for SH polynya area timeseries, by month, for the satellite products and JRA-CESM to further evaluate similarities and differences

Deleted: NOAA and OSISAF

Deleted: across the three grids (EASE, regridded daily, and monthly averages of regridded daily), the magnitudes show quite a large range, with the lowest correlations seen in the NOAA timeseries between the two regridded data (daily vs monthly). Correlations are generally highest during the late winter and [6]

Deleted: lower

Deleted: between the CDRs () than within the CDR () for

Deleted: most months and grids (spatial, temporal) and SH polynya areas identified in the NOAA and OSISAF monthly data on the 1° model grid are not significantly correlated for either April or October....

significant, are ~ 0.7 (area) to ~ 0.75 (N), suggesting considerable variability in the time series due to the nuances of the retrieval algorithms.

925

Correlations

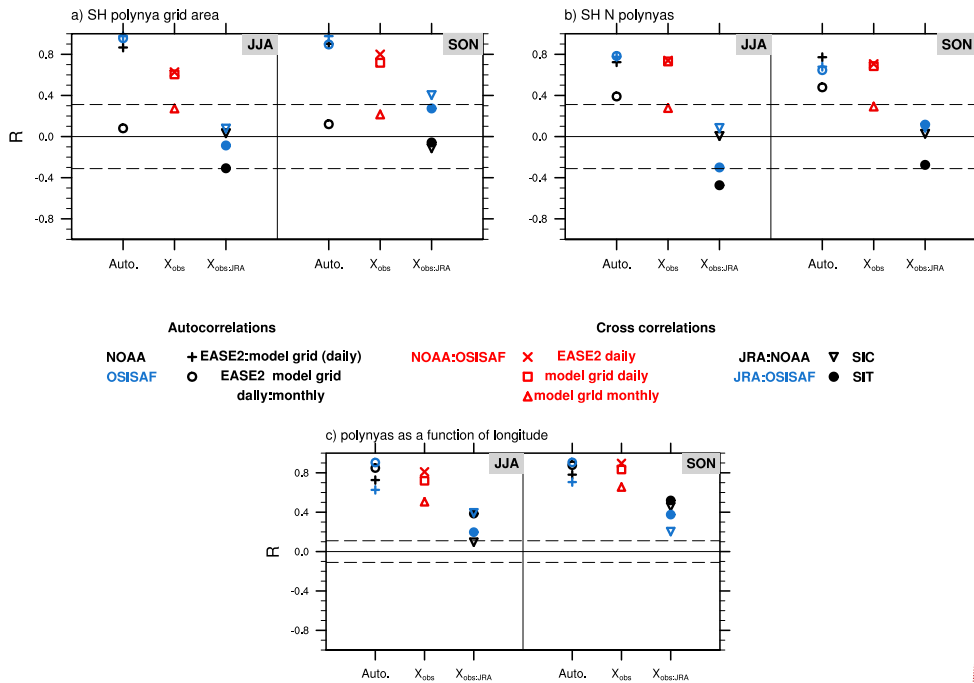
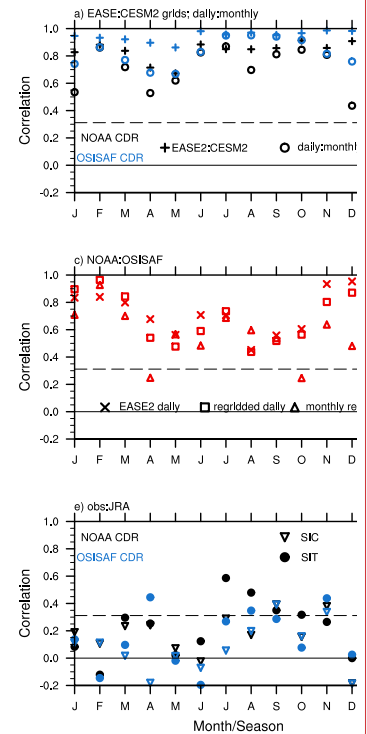


Figure 5. Correlation coefficients for integrated SH polynya areas (a), number of polynyas (b) and polynyas as a function of longitude (c) for each JJA (left) and SON (right). Autocorrelations are calculated between different grids (“regridding”) for same observational product (NOAA black; OSISAF, blue); cross-correlations between the two observational products (NOAA:OSISAF, red) and between the observational products and the JRA-CESM (obs:JRA; NOAA black; OSISAF, blue). Symbols show correlations between time/longitude polynya time series from the daily observational data on the original EASE grid vs daily (+) and monthly (o) regridded on the model grid; NOAA:OSISAF on the EASE grid (x) and then regridded daily (□) and monthly (open triangles); and between JRA-CESM polynyas identified using SIT 0.4 m (*) and SIC 85% metric (inverted open triangles). Dashed horizontal

930

Deleted: 0.75 for all grids from April to October,

Deleted: Curiously, integrated SH polynya areas estimated using the NOAA CDR on the original grid have significant negative trends in November, however not in the regridded product (Figure 5 and Table 1), whereas November SH polynya area trends are significant and negative across all three OSISAF polynya areas (EASE, daily regridded, monthly regridded). Indeed, there are significant negative trends in the OSISAF SH polynya area timeseries for all months except December; in the NOAA-derived polynya time series. [7]



Deleted:

Deleted: (left column) and trends (right column)

Deleted: month of the year and the annual average

Deleted: Correlations

Deleted: the NOAA and OSISAF data (a), between the NOAA and OSISAF data (b), and between the NOAA, OSISAF and JRA-CESM (all monthly and on the nominal 1° grid; (c). Plus (+) symbols in (a) indicate correlation coefficients between polynyas identified using the CDR on the EASE grid and regridded to the model grid, and open circles mark correlation coefficients between regridded monthly and daily data (NOAA correlations shown in black, OSISAF shown in blue). Mid [8]

lines in a-c indicate the 95% significance level based on the Mann-Kendall non-parametric trends significance (Mann 1945; Kendall 1975; and Gilbert 1987).

990

4.2.2 Regional polynyas in the satellite data

Winter (JJA) and spring (SON) polynya areas as a function of longitude show both similarities as well as differences resulting from choice of CDR (NOAA vs OSISAF), temporal (daily vs monthly) and spatial grids (EASE vs model; Figure 6). Higher polynya areas are identified, for example, by the NOAA data in the Ross Sea region and near the Antarctic peninsula in the OSISAF product. In general, polynya areas identified using the regrided daily product are higher in both CDRs than those identified using the daily data on the EASE grid or the monthly regrided data.

995

Latitudinal mean coastal polynya area (1979-2020)

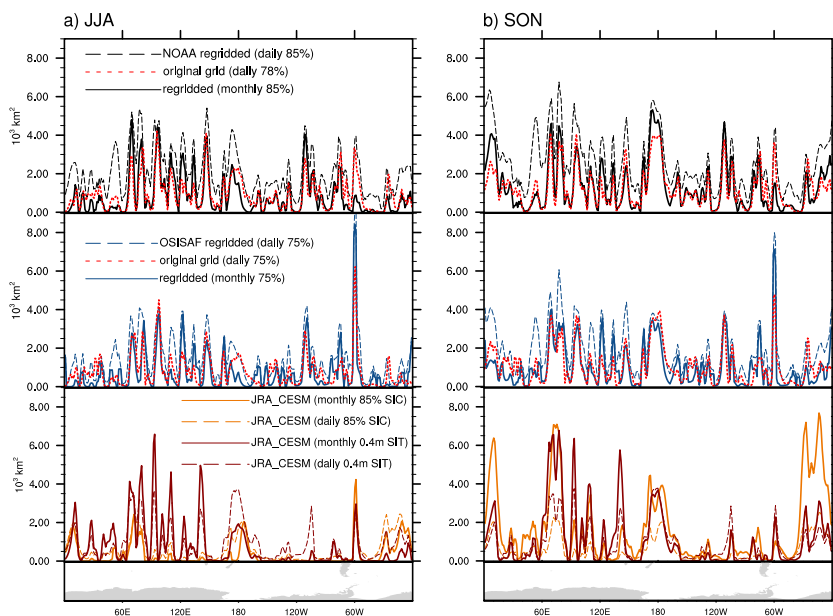


Figure 6. Winter (JJA; a) and summer (SON; b) mean coastal polynya area as a function of longitude for the NOAA CDR (top), OSISAF CDR (middle) and JRA-CESM (bottom). Polynya area as a function of longitude is shown as a 3° (longitudinal) running average. Top and middle panels show polynya areas for the three different grids and metrics - daily NOAA (78% SIC) and OSISAF (75% SIC) on the original grid (red dotted lines), CDR daily data regrided onto the CESM grid (NOAA 85% SIC black and

1000

Deleted: Significant trends (b,d,f) are indicated by the gold stars.

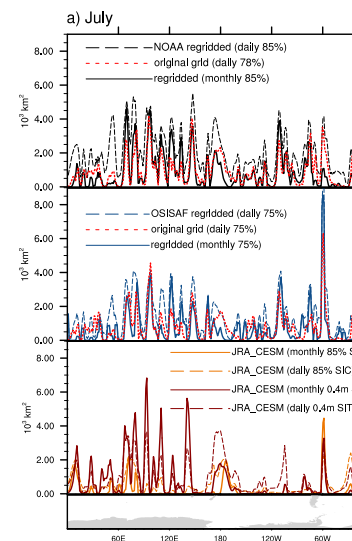
Deleted: in November,

Deleted: near the Antarctic peninsula in November and particularly in July

Deleted: - the exception to this is the Ross Sea in November, when higher polynya areas are identified in both products using the monthly, regrided data

Deleted: November sea ice is both highly variable and rapidly retreating (Fig. 1c), and the Ross Sea polynya often merges with the open ocean during November (not shown) - polynya areas identified using daily data can become "open water" overnight and the daily polynya area will suddenly drop, whereas the monthly averages may capture, on average, a higher polynya area due to smoother seasonal transitions of the ice pack resulting from monthly averaging.

Latitudinal mean coastal polynya area (1979-2020)



Deleted:

OSISAF 75% blue) dashed lines, and regrided and monthly averaged (NOAA 85% SIC, black and OSISAF 75%, blue) solid lines. Bottom panels in a) and b) show polynya areas based on JRA-CESM model simulation using different polynya thresholds: monthly (solid lines) and daily (dashed lines) SIC at 85% threshold (orange) and monthly SIT at 0.4m (brown) thresholds.

Regridding and monthly averaging SICs from the CDRs has lower impact on spatial auto- and cross correlations than on the SH integrated temporal correlations (Figure 5c). Climatological, coastal polynya areas as a function of longitude from the OBS data products show significant auto- and cross correlations regardless of temporal resolution or grid, and are generally higher than the temporal correlations. Unlike the temporal autocorrelations, the longitudinal autocorrelations are higher for polynyas identified on the monthly-averaged regrided data than for the daily regrided data.

Cross-correlations on regionally integrated timeseries are significantly correlated between the two observational data sources after regridding and monthly averaging only in the winter season in the Bellingshausen-Amundsen sea and the Indian sector ($R \sim 0.4-0.5$, respectively). In all other regions and in these regions in the spring, polynya areas and numbers estimated from the regrided and monthly averaged observational data products are not significantly cross correlated (Supplemental Fig. 9). Autocorrelations tend to be higher for polynya areas rather than polynya numbers, and the NOAA autocorrelations after regridding and monthly averaging (original EASE grid, daily: model grid monthly) are insignificant for all seasons and regions, except winter in the Bellingshausen-Amundsen sea.

Regional trends in polynya areas, when significant, are generally negative for both seasons with the exception of the Indian Pacific sector, which has only significant positive trends at high SIC thresholds for both seasons, and in the Indian sector where significant trends are generally positive in both NOAA and OSISAF for SIC thresholds below $\sim 80\%$ (JJA) or 55% (SON), and significantly negative in the OSISAF at SIC thresholds above $\sim 80\%$ (JJA)/ 73% (SON; Supplemental Figures 4-8).

4.3 Polynyas in the JRA-CESM vs NOAA and OSISAF OBS

4.3.1 Integrated southern hemisphere polynya area

Polynya-like features have been found in CESM2 (DuVivier et al., 2021; Singh et al., 2020), and the CESM2 reproduces many characteristics of Antarctic sea ice quite well, making it a suitable model for closer investigation of polynya-like features. Polynyas identified in the model and the observations may disagree if the model doesn't adequately capture mechanisms for producing polynyas, or due to model bias, or both. It is also possible that identification of polynyas in model output may require different metric choices than those used to identify polynyas in satellite products due to differences in model vs satellite data as outlined above.

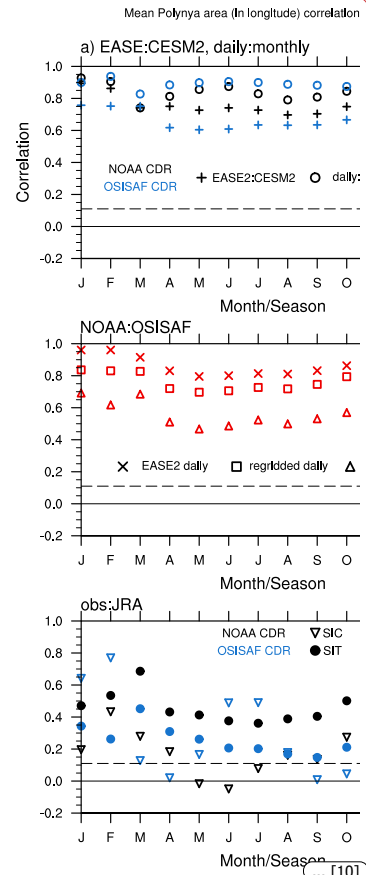
Polynya maps for the example day, July 15, 2003, show how the 85% SIC threshold identifies far fewer polynyas in the JRA-CESM than either the NOAA or the OSISAF CDRs (Fig. 2), suggesting that SIC may not identify polynya-like features in

Deleted: for all months across geographic (EASE, regrided) and temporal resolutions (daily and monthly), although regridding from the original EASE grid onto the 1° model grid lowers the regional correlations for the both products and particularly for the OSISAF, April-October. (Figure 7).

Deleted: Furthermore, longitudinal correlations between the monthly regrided CDR (NOAA:OSISAF) products lie between 0.4 and 0.6 for fall through early spring (April through October), and correlations between the OBS are generally lower than they are within an observational product, highlighting that both regridding (geographical and temporal) and different retrieval algorithms can result in different regional polynya identifications. Correlations of regional timeseries of polynya areas give more insight into ... [9]

Deleted: ure

Deleted: All other sectors have multiple months and/or grids when regional timeseries from the two OBS are not significantly correlated – in fact 20% of the time the regional polynya timeseries from the regrided monthly data are not significantly correlated (Figure 8). Temporal correlations between the two OBS in regional polynya timeseries are particularly lower in the Weddell and Pacific sectors in the spring-winter (Wedell; April-August) and winter (Pacific; July-August), respectively.†



Deleted: ... [10]

Deleted: Polynyas identified in the Ross Sea region in July and both the Ross and Weddell Sea regions in November show significant declines in area 1979-2020 for both OBS, however only in the polynyas identified on the original EASE grid for the NOAA CDR. If all months of the year are considered, trends are significant and consistent in both OBS from April through November/September for the Ross/Bellinghausen-Amundsen Sea (Supplemental Figures 7-11). Strikingly, trends are significant ... [11]

Deleted: Variability in SH polynya areas tends to be larger during the ice retreat season November-January) in both OBS and the JRA-CESM, and SH polynya area for a given SIT threshold value are largest in November (Fig. 3b and Supplemental Figs. 3-4).†

135 model output in the winter season. Indeed, monthly climatological (1979-2020) wintertime (JJA) SH polynya areas remain very small in the JRA-CESM across the full range of SIC thresholds (Fig. 3; summer and fall are shown in Supplemental Fig. 3). During freeze up through winter, open water can freeze very quickly in the model, resulting in high SICs and yet relatively thin SITs. Monthly climatologies of SH polynya area reveal that SIT thresholds identify large areas of wintertime coastal polynyas across a range of SIT thresholds, unlike SIC thresholds (Fig. 3). Both the integrated SH polynya areas and numbers

140 are nearly the same regardless of whether they are identified in the model output using daily or monthly data.

To compare with polynyas identified in the observational products, we use polynyas identified in the JRA-CESM using thresholds of 85% SIC and 0.4m SIT (and we show results in Supplemental Figures 12-13 using a SIC threshold of 50% SIC and SIT of 0.2 m for comparison). Figure 4 shows time series of SH polynya area and total number of SH polynyas for winter and summer, and underscores many of the complications comparing polynyas estimated from satellite products to those estimated using climate model output on a seasonal basis. There are significant seasonal differences in polynyas identified using these two metrics: polynya areas identified using the SIT metric are roughly three times as large as those identified using the SIC metric (and much closer to the SH polynya areas in both OSISAF and NOAA CDRs) for winter (JJA), whereas the magnitude of SH polynya area is similar using these thresholds in the spring (SON; Figure 4). Fewer discrete polynyas are identified in the JRA-CESM using both SIT and SIC metrics than in either observational product in both seasons, even though the polynya areas are similar and thus the average polynya size will be smaller in the observations than in the model.

145

Temporal cross-correlations for SH polynya area, 1979-2020, between the NOAA, OSISAF and JRA-CESM are significant only between the OSISAF and the JRA-CESM using the SIC metric in the spring (SON; Fig. 5) – although it is interesting to note that the cross correlations between regrided, monthly NOAA and OSISAF polynya area or number time series are not significantly correlated in either season. Trends (1979-2020) in SH polynya area in the JRA-CESM are significant and negative only for the polynyas identified by the SIT metric, and for a limited range of thresholds in both winter and spring (Fig. 3).

4.3.2 Regional polynya areas

160 Integrated mean SH polynya areas are very similar between the observational and model data for the metrics used, yet there are subtle regional differences. For example, climatological integrated SH polynya areas show very little difference whether using daily or monthly data (e.g. Figure 3), and yet the longitudinal maps reveal that the daily SIT data identify more wintertime polynyas than the monthly SIT data in the Ross and Bellingshausen-Amundsen seas (Fig. 6). Wintertime polynyas in the Bellingshausen-Amundsen sea are particularly anemic using the 85% SIC metric (daily and monthly). In contrast, in spring (SON) the SIC threshold identifies higher modeled polynya areas in this region and they are closer to the polynya areas identified in the NOAA and OSISAF. Similar to the cross-correlations between the polynyas in the observational products, spatial cross-correlations between polynyas in the model and the observations are higher than temporal ones. Spatial cross correlations between polynya area as a function of longitude identified in the satellite products and the JRA-CESM polynya

Deleted: for fall through mid-winter

Deleted: 3e and Supplemental Fig. 5

Deleted: throughout the fall and winter

Deleted: e and Supplemental Fig. 5

Deleted: Comparing polynyas identified in the satellite observations and the model output, we find that on a climatological, hemispheric basis, the best correspondence between SH polynya areas identified in the model and the observations differ by month: model simulated polynya areas identified using a 0.4 m SIT threshold correspond well to the observations in late fall through early spring (April-October), whereas SIC of 85% in the model output for late spring months (November) more closely correspond to those from the satellite product. Variability in the SH polynya area is highest in December and January (Supplemental Figs. 3-5), when Antarctic sea ice is rapidly retreating (Fig.). The smallest polynya areas across all thresholds in the JRA-CESM, as in the CDRs, are found in February and March, when sea ice is at a minimum then beginning its seasonal expansion.

Deleted: The metrics and thresholds that identify similar integrated SH polynya areas in the JRA-CESM to observationally based estimates are a SIT of 0.4 m and SIC of 85%.

Deleted: both SIT and SIC metrics

Deleted: in the model output

Deleted: Interestingly, the mean and variabilities in November SH polynya areas in the JRA-CESM identified using SIC more closely match those in the NOAA timeseries than those using the SIT, which more closely match the mean and variability in the OSISAF SH polynyas (Figures 4-5, Table 1 and Supplemental Figure 6).

Deleted: monthly OBS

Deleted: a few months of the year – namely July-October using

Deleted:

Deleted: the 0.4m SIT threshold for the NOAA timeseries, and the months of April (SIT 0.4m), August (SIT 0.4m) and September (SIT 0.4 m, SIC 85%) for the OSISAF timeseries (Figure 5e). On an annual basis, correlations are positive and significant with both OBS however only for the SIC threshold in the JRA-CESM. Correlations between SH polynya timeseries in July/August between the SIT-based JRA-CESM polynyas and the NOAA CDR ($R=0.59/0.48$) are nearly as high as the correlations between the monthly OBS (NOAA-OSISAF; $R=0.69/0.60$). The number of discrete polynyas identified in the satellite products are 2-3 times as numerous as those identified in the model output, and thus larger, except during the summer months (DJF) when the number of discrete polynyas in the OSISAF and the JRA-CESM using SIT as a metric are similar ((Figure 5, Table 1 and Supplemental Figure 6). Thus, polynya (... [12])

Deleted: s

Deleted: , as they are in the OBS, however they are significant only in the SIT in July- August, and in both SIT and SIC de (... [13])

Deleted: Polynyas in the Bellingshausen-Amundsen sea region tend to be anemic compared to the OBS in winter (July), wi (... [14])

Deleted: November

Deleted: The monthly 0.4 m SIT threshold identifies larger areas of polynyas in the Pacific than those identified in the satellite (... [15])

area significant and positive for both metrics (SIT, SIC) and both observational products (NOAA, OSISAF) in the spring (SON), and SIT (NOAA, OSISAF) and SIC (OSISAF) in the winter (JJA; Fig. 5).

Deleted: (Fig. 7) are higher than the temporal correlations for the integrated SH timeseries (Fig

Regional trends are generally not significant in the model for most SIT and SIC thresholds (Supplemental Figs 4-8), although there are some regionally significant trends for the SIT (0.4) metric, both negative (SIT: Ross, JJA; Weddell JJA and SON) and positive (SIT: Bellingshausen-Amundsen Sea, SON) as well as significant negative trends in wintertime Indian sector polynyas identified using the SIC metric.

4.4 Impacts of different definitions for sea ice concentrations in the model and satellite data

Discrepancies between polynyas identified using SIC in the model and the observational data may arise due to differences in SIC definitions in satellite-based versus model data, particularly during the winter months. As discussed above, sea ice can form immediately in the model during the cold austral expansion season and through the winter, thus resulting in SICs that are high even though the ice may be very thin. Satellite imagery cannot differentiate between water and sea ice at very low SICs or low sea ice thicknesses. To understand potential impacts that these model and observational differences in SICs may have in polynya identification metrics, we degrade the model SIC output to more closely mimic satellite estimates of SIC. In areas of low (<10% SIC) or thin (<5cm SIT) ice, we set daily SICs to 0% SIC, and in thin ice areas (5-20 cm SIT) the originally modeled SICs are reduced by half. We then identify polynyas using an 85% SIC threshold on the degraded model output.

Deleted: quite varied in sign, magnitude and season across all data sources (Table 2 and Supplemental Figures 7-11). Regional polynya area trends (1979-2020) are insignificant for most months in both the SIT and SIC identified regional JRA-CESM timeseries, with a few exceptions. Trends are significant and negative in the Indian sector in July (SIT and SIC metrics) and on an annual basis using the SIC metric. Significant regional trends are found in both of the OBS and one of the JRA-CESM polynya timeseries (SIT or SIC) for only two regions and months – in the Ross Sea in March (Supplemental Figure 11), and the Pacific Sector in October (Supplemental Figure 10). Although all three polynya timeseries (NOAA, OSISAF, and JRA-CESM using SIT) show significant negative March trends in the Ross Sea, two show significant positive (NOAA and JRA-CESM using SIC) and the other significant negative (OSISAF) October trends in the Pacific Sector. In August in the Indian sector, however, both JRA-CESM polynya timeseries have significant negative trends, whereas the NOAA polynyas have significant positive trends, and the OSISAF do not have significant trends. One possible source of differences in trends between the hindcast model output and the satellite-based products may lie in the reanalysis product used to force the CESM-JRA, discussed in section 5 below, although differences in trends between the OBS also suggest high uncertainties in many regional polynya trends.

Comparisons of the standard model to degraded output indicate that degrading SICs results in small, positive differences that are largest within the ice pack during ice growth season and along the ice edge in the winter (Fig. 4 and Appendix C); differences from degraded output during the sea ice retreat season (SON) are much smaller with no discernible patterns (not shown). Degrading the model data results in lower SICs throughout much of the fall pack ice and along the winter sea ice edge, and these differences show very little regional variability and do not consistently explain the model bias of the non-degraded data compared with the satellite products and in some cases would further increase model-observational biases. Identifying polynyas based on the degraded model data (using an 85% SIC threshold) results in an increase in wintertime polynyas by ~10-20% (Figure 4 and Supplemental Figures 12,13). This increase is quite small compared to the model (using the SIC threshold) versus CDR polynya area differences. Thus, it does not explain the differences in polynya areas estimated from these three products and we focus on results using the standard model output (non-degraded) for the remainder of this paper.

Deleted: wintertime

Deleted: identification

Deleted: and Supplemental Figs. 4-5

Deleted: (Supplemental Figs. 4-5)

Deleted: fall and

Deleted: 12

Deleted: 13

4.5 Relationships between polynyas and NPP in the JRA-CESM

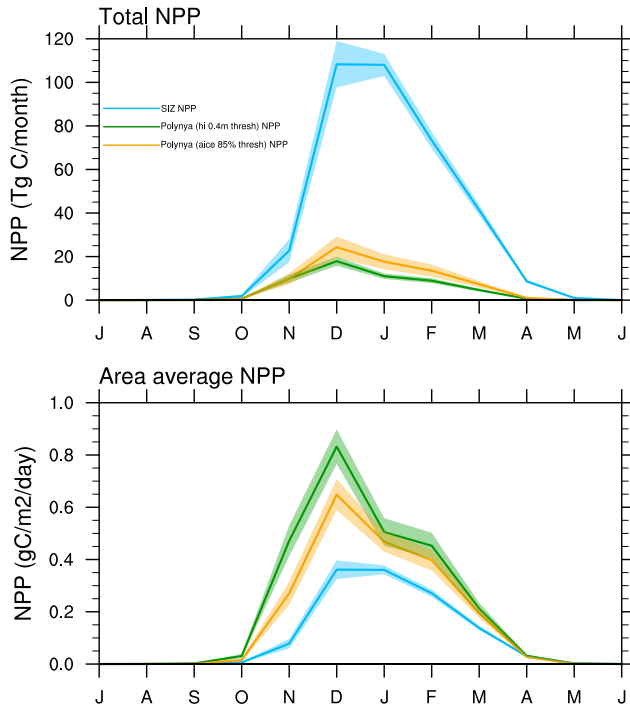
Net primary productivity (NPP) describes the rate of photosynthetically fixed carbon in the upper ocean; it quantifies the energy available for marine food webs. In the high-latitude Southern Ocean, NPP increases markedly as the sea ice retreats and light returns to Antarctic waters (e.g. Richert et al., 2019 and references therein). Light reaches the surface sooner in polynyas than the surrounding ice-covered areas, relieving phytoplankton of light limitation (e.g. Arrigo & van Dijken, 2003).

315 We look at polynya regions defined in the austral spring (SON), to see if the model captures high NPPs within identified
polynyas during the early growth season as is found in observations. The choice of metric (concentration or thickness) to
identify SON polynyas in the model is not clear based on the previous analysis that indicates not only differences between the
two OBS w.r.t. polynya areas, temporal and spatial correlations and trends, but also that polynyas identified in the JRA-CESM
using a 0.4 m SIT and 0.85% SIC thresholds each have seasons and/or regions that better correlate with the NOAA or with the
1320 OSISAF. We therefore use austral spring polynya regions as identified by both the 0.4 SIT and the 85% SIC metrics for the
NPP analysis.

Deleted: September, October, November, “

Deleted: months

Comparing the monthly average NPP per unit area within austral springtime coastal polynyas and within the sea ice zone
allows us to better understand how polynyas may augment austral spring NPP and thus play a critical role in the Antarctic food
325 web (Figure 7). Note that the SIZ, which is defined as the area covered seasonally with sea ice (as determined by the mean
winter - JJA - 85% SIC contour) covers significantly more ocean area than the spatial area of polynyas, so the overall
production within the SIZ is larger than in polynyas (Figure 7, top). However, we find that the NPP per unit area is substantially
higher during the austral spring in regions identified as polynyas using both SIC and SIT polynya identification methods than
it is within the SIZ generally (Figure 7, bottom). This finding suggests that the model does indeed capture high productivity
330 within low and/or thinner ice regions. Additionally, the higher NPP per unit area persists into the summer and early spring
(December-March) as well. Polynyas have a particularly large impact on NPP during December, when area average NPP
within polynyas is more than twice as much as within the SIZ when using the 0.4m SIT threshold and 1.5 higher when using
the 85% SIC threshold. Although the total integrated SON polynya area is an order of magnitude smaller than the total SIZ
area, NPP within polynyas contributes ~17-23% of the total NPP during the December peak. These results highlight that
335 polynya-like features are playing an important role in Antarctic marine productivity in the CESM2.



340 **Figure 7.** JRA-CESM 1979-2020 climatological integrated SH monthly total NPP (top) and area-averaged NPP (bottom) for the sea ice zone (SIZ: blue) and SON polynya regions identified using 0.4 SIT (green) and 85% SIC (orange) thresholds.

5 Discussion

345 Polynyas are often qualitatively defined -- “open water surrounded by ice and/or ice and land” -- and a leading conclusion of this work is that care must be taken when identifying quantitative polynyas data from gridded products. Polynyas are a feature of the sea icescape – a complex, dynamically changing structure that is an integrated component of polar marine ecosystems as well as a leading player in polar oceanic and atmospheric circulations and dynamics.

Deleted: 9

Deleted: 4.6 CESM2-LE: Antarctic coastal polynyas and NPP in a changing climate

The above analysis indicates that the JRA-CESM is simulating polynya-like features with elevated NPP compared to the SIZ. We extend our analysis to the fully-coupled 50 member CESM2 Large Ensemble (CESM2-LE) over the historical (1850-2014) and future moderately-high emission (SSP370) scenario (2015-2100) to explore how polynyas and NPP may change in a changing climate (Figure 10). SH coastal polynya areas identified in the CESM2-LE using both the SIT 0.4m and SIC 85% thresholds indicate that polynya areas tend to be higher in the fully coupled CESM2-LE during July using the SIT threshold, as was found in the JRA-CESM simulations, and the same size in November for both metrics until the mid-1900s, when SH polynya areas identified using SIC start to decline. Simulated polynyas in the hindcast simulation (JRA-CESM) tend to lie on the high side of the CESM2-LE range and more than 1 standard deviation above the 10-year running ensemble mean for both SIT and SIC thresholds in both July and November, indicating the influence of the reanalysis atmospheric forcing. Polynyas estimated from both OBS fall within the range of the SIT-based July polynyas in the CESM2. In November, NOAA-polynyas lie within the SIC-range, whereas OSISAF polynyas lie within both SIT and SIC identified polynya ranges in the CESM2-LE. The number of discrete wintertime coastal polynyas identified in the observational products is significantly larger than from either polynya metric in the model simulations in July, although in November the numbers of polynyas in the NOAA time series is more closely aligned with polynya numbers in the model (Figure 10). SH CESM2-LE July polynya areas identified using the SIT threshold show small increases from 1850-2100 (Fig. 10a). November SH polynya area decreases in both the SIT- and particularly in the SIC-identified areas over the last 40-50 years of the 21st C (Fig. 10b).

... [16]

Deleted: quantitatively

Deleted: data

Ideal metrics and thresholds for polynya identification will depend on the product grid sizes, region of interest, season and scientific application, as well as the specifications of an individual data product. Many coastal polynyas occur on smaller scales than can be resolved by the original EASE grids of the satellite-based SIC products much less the typical nominal 1° grid of ESMS. An important result of this work is that although grid size may preclude resolving many individual polynyas (particularly many coastal polynyas), “polynya-like features“ may indeed be identified.

Gridded SICs retrieved from satellite images reveal much about the sea icescape, yet different retrieval algorithms can result in extremely small differences in hemispheric and regional integrated sea ice extents and areas and simultaneously significant differences in temporal variability, correlations and trends in sub-grid scale features, as shown in this analysis of polynyas identified using SIC thresholds. These differences may be partially due to the difficulty of capturing areas of low SICs and/or low SITs through remote sensing, although disentangling the sources of these discrepancies is beyond the scope of this work. That the same passive microwave data but different retrieval algorithms can lead to uncorrelated timeseries of SH polynya areas and numbers once the data have been regridded and monthly averaged by is remarkable. Polynya areas identified in both observational products are, however, significantly correlated spatially (longitudinally), regardless of spatial (EASE vs model) and temporal grids (daily vs monthly). This result suggests that on a climatological scale, locations of polynya-like features identified in both observation products are consistent even if their temporal variability, correlations and trends are not. The CESM2, like many ESMS, does not simulate land fast ice and therefore landfast ice cannot serve as anchors for coastal polynyas in the model. This may help explain the somewhat smaller cross-correlations between polynyas in the model with polynyas in the observational products compared to the cross-correlations of NOAA and OSISAF polynyas.

Inconsistencies between identified polynyas in these two observational products complicate comparisons with ESM output, which are typically on coarser grids and daily or monthly averages rather than daily snapshots. Polynya features identified within both observational products and the JRA-CESM are consistent in terms of climatological means and geographic locations, even as temporal correlations, variabilities and trends are inconsistent between all of the products (when on the same grid). The highest spatial (longitudinal) cross-correlations between the JRA-CESM and NOAA polynyas are nearly as large as cross-correlations between the two observational products (after regridding). The JRA-CESM successfully simulates polynya-like features in the icescape along the Antarctic coast, in a manner that is spatially consistent with both the NOAA and the OSISAF products, although the JRA-CESM tends to simulate lower polynya areas in the Bellingshausen-Amundsen sea than those estimated from the either product. Polynya-like features identified in the JRA-CESM show significantly higher NPP in these features identified using both SIT and SIC thresholds, than in the larger sea ice zone, and thus this method of identifying polynya-like regions successfully identifies biological hotspots in the model: NPP within polynyas in the JRA-CESM contributes to about 18% of the total Antarctic SH marine NPP even though the sea ice zone is roughly ten times as large as the springtime coastal polynya areas.

Deleted: Sea
Deleted: ice concentrations

Deleted: , but areas of
Deleted: such as polynyas are difficult to capture

Deleted: OBS
Deleted: for all months and annually

Deleted: however R values are relatively low (~0.5) for April through October considering both the OBS use the same base data and differ only by retrieval algorithm. Temporally integrated SH polynya areas are significantly correlated, although with lower R values in general than the spatial correlations. This is true both within an OBS (e.g. NOAA EASE: NOAA regridded) and between the OBS (NOAA:OSISAF) for all months and grids, except for April and October. Differences in polynyas identified in the two OBS suggest a sea icescape complexity that may not be fully captured by SIC retrieved from satellite imagery. ¶

Deleted: (SIT)
Deleted: from April-October

Deleted: they are between
Deleted: and the JRA-CESM SH polynya area (based on SIT metric) is significantly correlated with the OSISAF/NOAA in April/October. Results from t

Deleted: indicate that the model is
Deleted: simulating

Deleted: CDR
Deleted: T

Deleted: the NOAA or OSISAF
Deleted: indicates that marine NPP, on average, is approximately twice as high within polynya areas as within the sea ice zone as a whole.

We provide some “best practices” from this systematic comparison of polynya identification methods in satellite-based and the CESM below, and discuss the implications of polynya metric choices for applications in climate models.

5.1 Polynya metric choices: Temporal and spatial resolutions

Analysis of polynyas identified in both satellite and model products suggest that integrated SH climatologies made from daily vs monthly data do not differ significantly, and thus monthly data may be sufficient for some analyses on longer temporal scales. Integrated polynya (area and number) timeseries auto- and cross-correlations are reduced when regriding the observational SIC data, to the point that regrided (from EASE to model grids) monthly data from the two observational products are not significantly correlated – yet the spatial cross-correlations remain significant even after regriding between the two products. Thus, the method used here identifies polynya-like features that are geographically consistent between the two regrided observational products and yet inconsistent in temporal variability. We therefore recommend that in order to eliminate discrepancies due to grid types and resolutions alone, we recommend comparing metrics from data on the same grids (temporal and spatial), and regriding - if necessary - data with the higher geographical resolution onto the coarser resolution grid. Trends in polynya areas are not robust – including in sign, magnitude and sign – across the range of SIC thresholds, grids and product sources (retrieval algorithms) in the observations analyzed here. These inconsistencies between temporal variabilities, cross-correlations, and trends, and consistencies in geographical cross-correlations between polynyas in the two observational products suggest that the observational products may serve as good (poor) sources of verification of polynyas in ESM data spatially (temporally).

5.2 Polynya product and metric choice in modeled data

Using SICs, in general, to identify SH wintertime coastal polynyas in model simulations requires very high thresholds and is particularly problematic in the Bellingshausen-Amundsen Sea. Part of this issue is likely because ocean surface waters can very rapidly refreeze and form very high sea ice concentrations in all models, not just the CESM. Degrading model output to more closely resemble satellite estimates of SICs leads to only small increases in polynya areas identified using SICs (at 85% threshold) and does not explain the large bias between polynyas identified in winter (JJA) in both observational products and the JRA-CESM. We thus find that identification of wintertime polynyas in the CESM better reproduces observed polynyas when using a SIT-based threshold, which more accurately accounts for low sea ice areas than SICs, which can be very high in the model even in very thin sea ice conditions, unlike in satellite imagery. We suggest using a SIT-based metric for wintertime coastal polynya identifications in model output.

It is interesting to note that while significant longitudinal correlations exist between polynya areas identified in the CESM-JRA and the OBS for each month of the year and annually (Fig. 4c), the same cannot be said for temporal correlations of the integrated time series (Figs. 5c and 6a-e). This suggests that the regionality of the identified polynyas in the CESM-JRA is captured well compared to the observations, however the temporal variability is less well captured in some regions and seasons.

Deleted: The fully coupled CESM also has polynya-like features with relatively high NPP. Integrated polynya area in the CESM2-LE tends to be lower, on average, than in the JRA-CESM, 1979-2020, although the polynya area in the JRA-CESM fall within the spread shown by CESM2-LE during the historical period. NPP within polynyas remains high and relatively unchanged over the 21st century in the CESM2-LE under the SSP370 emissions scenario, although the contribution of NPP within polynyas to the total SH NPP is lower by 2100 primarily due to overall increases of NPP in the sea ice zone.

Deleted: many

Deleted: both from observations and climate model output

Deleted: larger

Deleted: In general, polynya areas defined by the same SIC threshold and product will be slightly larger using daily data than monthly data for the NOAA CDR. There are seasons and regions, however, that show significant differences in polynya areas between daily data and monthly data at the same threshold value in different data products, and when monthly data may lead to larger polynya area identification – e.g. in the Ross and Weddell Seas from late spring through late summer (November-March). Daily SIT data in the model, however, leads to higher polynya areas than monthly data in the Ross and Bellingshausen-Amundsen seas.

Deleted: July by the OBS

Deleted: using 85% SIC thresholds

Deleted: A more direct comparison between SICs as a metric to identify polynyas in both simulated and observed data could be made with the use of a satellite-simulator in the model to calculate brightness temperatures as a satellite would measure them (e.g. Smith et al., 2021). Wintertime polynya-like features are identified in the CESM using daily SICs along the eastern Antarctic coast, and yet not in the Bellingshausen Sea (e.g. Fig. 4) suggesting that there may be model biases in the CESM impacting regional sea ice dynamics.

Deleted:

1555 Part of this may be explained by the reanalysis data used to force the CESM-JRA and the nature of coastal polynyas. Reanalysis wind products show the lowest biases compared with weather station data in regions and times of high synoptic and/or low katabatic wind activity, and significant biases in wind fields close to the coast near where katabatic winds significantly impact coastal winds (e.g. Jones et al., 2016; Harrison et al., 2022). Katabatic winds are integral to the formation of coastal polynyas (e.g. Thompson et al., 2020 and references therein). Thus, coastal polynya variability due to variability in katabatic winds may
1560 be captured by the polynya time series in the observations but not well represented in the atmospheric reanalysis data used to force the model.

Recent work found significant positive trends in annual polynya areas in the Ross, Weddell, Indian and Pacific sectors estimated using daily data from the OSISAF CDR product at a 50% threshold on the 25 km x 25 km EASE grid (Duffy et al.,
1565 2023). Our results show significant positive polynya area trends in the OSISAF on the EASE grid only in the Indian sector (JJA and SON) and integrated across the SH (JJA) with a 50% SIC threshold. These contradictions may be due to differences in metrics or methods used to identify polynyas - an analysis beyond the scope of this work - yet it highlights that caution should be taken when comparing results from different sources, grids, methods and metrics. Indeed, one of our primary conclusions from this work is that trends of polynya-like features identified on grids that may not truly resolve distinct polynyas (as opposed to polynya-like features) should be viewed with caution, as different thresholds may result in even different signs of significant trends.
1570

5.3 Polynya applications: coastal polynyas and NPP in a changing climate

Our analysis with the JRA-CESM, demonstrates that the CESM is indeed capturing enhanced productivity within polynya-like features in austral spring compared to within the entire SIZ. Elevated rates of NPP occur in polynya features identified using either a 0.4 m SIT or an 85% SIC thresholds, with similar rates of productivity in SIC and SIT-defined polynyas. NPP within these polynya-like features contributes ~17-23% of the total sea ice zone NPP during the December peak, even though the area of these polynyas is only ~3% of the sea ice zone. This finding underscores how critical polynyas are for the base of the Antarctic food web, and using models to understand these areas is particularly critical given the challenges of satellite chlorophyll retrievals in these areas (e.g. Oliver et al. 2025).
1575

1580 6 Conclusions

The definition of “polynyas” in a quantifiable sense is relatively subjective. Defining areas and timing of open water within the Antarctic sea ice zone such that comparisons can be made between satellite based SICs and model output require careful consideration and recognition of the basic differences between satellite observations and model output. It is critical to consider grid type and resolution, season, metric and threshold as optimal metrics chosen may depend on region and season of interest.

1585 In summary, our conclusions w.r.t. our primary four questions are:

Deleted: summertime (DJF) in the Weddell Sea, summer (December) and fall (MAM) in the Indian sector, and summer-fall (DJFMAM) in the Pacific sector, and significant negative trends in the Bellingshausen-Amundsen Sea (Jan-Sept), the Weddell Sea (April-May; Oct-Nov), the Indian sector (Oct), the Pacific sector (Aug-Sept) and Ross Sea (April-November)

Deleted: 2-LE

Deleted: metric to identify polynyas in the austral spring (SON) result in larger ensemble mean areas of polynyas in the SIT-identified polynyas than in the SIC-identified ones

Deleted: Contributions to NPP are quite similar

Deleted: and polynyas identified using both metrics show substantial augmentation of Antarctic NPP within polynyas compared to within the entire SIZ, indicating that the CESM is indeed capturing enhanced productivity within polynya-like features in austral spring. Changes in NPP within polynyas are small compared to those within the SIZ, which increases substantially and changes seasonality by the end of the 21st Century. This analysis demonstrates that the CESM may be a useful tool to investigate changing Antarctic marine ecosystems within polynyas and the sea ice zone in a warming climate. As the climate warms and sea ice responds, better understanding how to identify polynyas in different regions or seasons will be critical for quantifying how production in the ocean around Antarctica may change including timing of peak NPP production, changes in trophic transfer and species composition, etc.

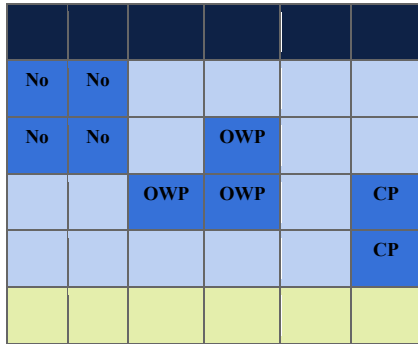
1. The JRA-CESM2 captures climatologically and biologically relevant coastal polynya-like features.
2. Complications from comparing polynyas identified from observational products to those identified from model output arise due to differences in grids and observational product sources (retrieval algorithms) and such that temporal variabilities and trends are inconsistent not only between polynya- features in the model and the observational products, but also between the two observational products.
3. Spatial locations of winter-spring coastal polynya-like features are consistent between both NOAA and OSISAF, and also between the JRA-CESM and both observational products.
4. Coastal polynya-like features in the JRA-CESM serve as biological hotspots, contributing ~17-23% of the total sea ice zone marine net primary productivity even while occupying only about 3% of the area of the sea ice zone, consistent with observational studies.

Appendices

Appendix A: Polynya algorithm

The polynya algorithm cycles through maps of the sea ice variable (concentration or thickness in this work) and initially labels any grid cells that fall below the threshold and that lie within the sea ice zone (south of the open ocean boundary). The algorithm iteratively cycles through the polynya maps to determine if grid cells that meet the threshold criteria are surrounded by sea ice and land (in which case they are labeled a polynya) or lie next to open ocean (in which case they are not identified as a polynya). Figure AA1 shows a schematic of a hypothetical region with land, ocean, sea ice and polynya grid cells. In this example, there are two polynyas – one open water polynya (occupied by three grid cells), and one coastal polynya (occupied by two grid cells). Figure AA2 shows an example satellite image of the Ross Bay and Terra Nova polynyas and grid cells labeled by SICs.

Deleted: primary recommendations are:
all data should be regridded to the same type and size of grid for comparisons to reduce differences due to grids alone
polynya areas identified from monthly and daily data are comparable on annually averaged, integrated hemispheric basis
sea ice thicknesses are a more suitable metric for identifying polynyas in climate model data in the winter months
sea ice concentrations are a more suitable metric for identifying polynyas in the late spring in climate model data, when sea ice is rapidly retreating, though this may be model dependent
optimal metric and threshold choices will be influenced by grids, regions, and seasons of interest
productivity within polynya areas may help evaluate model performance with respect to capturing enhanced productivity in polynya-like features, as seen in observations.



No = not polynya
OWP = open water polynya
CP = coastal polynya

	0% SIC (open ocean)
	< threshold (e.g. 50% SIC)
	> threshold (e.g. 90% SIC)
	Land

1650

Figure A1. Schematic of grid cells considered open ocean (dark blue), land (light green) and within the sea ice zone (light and medium blue). Grid cells in the sea ice zone that meet the threshold criteria are in medium blue; grid cells that lie above the threshold are in light blue. Grid cells that meet the criteria are identified as polynyas only if they are bounded by sea ice (open water polynyas) or sea ice and land (coastal polynyas).

1655

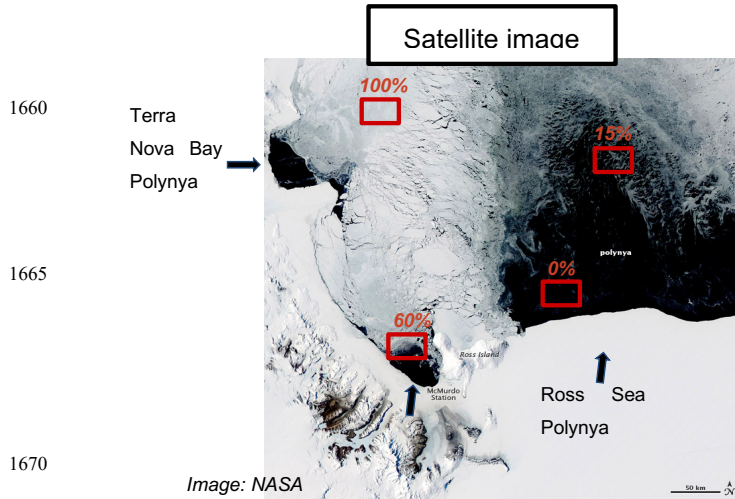


Figure A2. Example satellite image of the Terra Nova Bay and Ross Sea polynyas (Moderate Resolution Imaging Spectroradiometer (MODIS) image of the day from the National Aeronautics and Space Administration (NASA) Aqua satellite, November 16, 2011 https://eoimages.gsfc.nasa.gov/images/imagerecords/76000/76474/rosssea_amo_2011320_lrg.jpg). Hypothetical grid cells with SICs are shown in red.

Appendix B: Grid size and type and impact on polynya identification

Using concentration thresholds to define polynya regions will define how much open water (and likewise sea ice) is in the grid cell by percentage. For an Equal Area Scaleable Earth (EASE) grid this will correspond to an area that doesn't change with latitude or longitude, whereas on an equal latitude-longitude grid a SIC percent threshold will correspond to different areas of open water (or sea ice) depending on latitude. For example, a 50% sea ice concentration threshold on a 25kmx25km EASE grid corresponds to 312.5 km² or more of open water (and also 312.5 km² of sea ice) within the grid cell to meet the threshold requirement for a polynya. A grid based on latitude and longitude, which is common for earth system models, will have a varying range of surface area in each grid cell. A grid cell of ~3.2 10³ km² (about the area of grid cells next to the Antarctic coast on the Pacific and Indian sectors in the CESM) would have 312.5 km² of open water at a SIC threshold of 90%. Figure AB1 shows the area of the grid cells in the ocean grid in the CESM2 and areas of open water that would be contained in grid cells for example SIC thresholds. An example of the SIC thresholds required to result in 312.5 km² of open water within a grid are shown in Fig. AB2 for an equal area grid cell and two grid cells from a 1°x1° grid cell at two different latitudes. Different grids can also lead to different areas and numbers of polynyas even when the open water areas are the same (e.g. Fig. AB3).

Deleted: definitions

Deleted: or

Deleted: sea ice concentration at which a grid cell on the CESM grid (~1°x1° lat/long) will contain 312.5 km² of open water, or the same area of open water as on a grid cell on an EASE grid that has 50% SIC....

Deleted: sizes

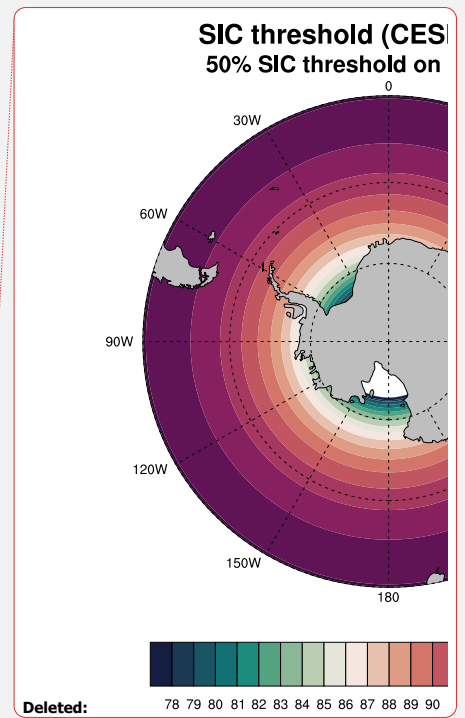
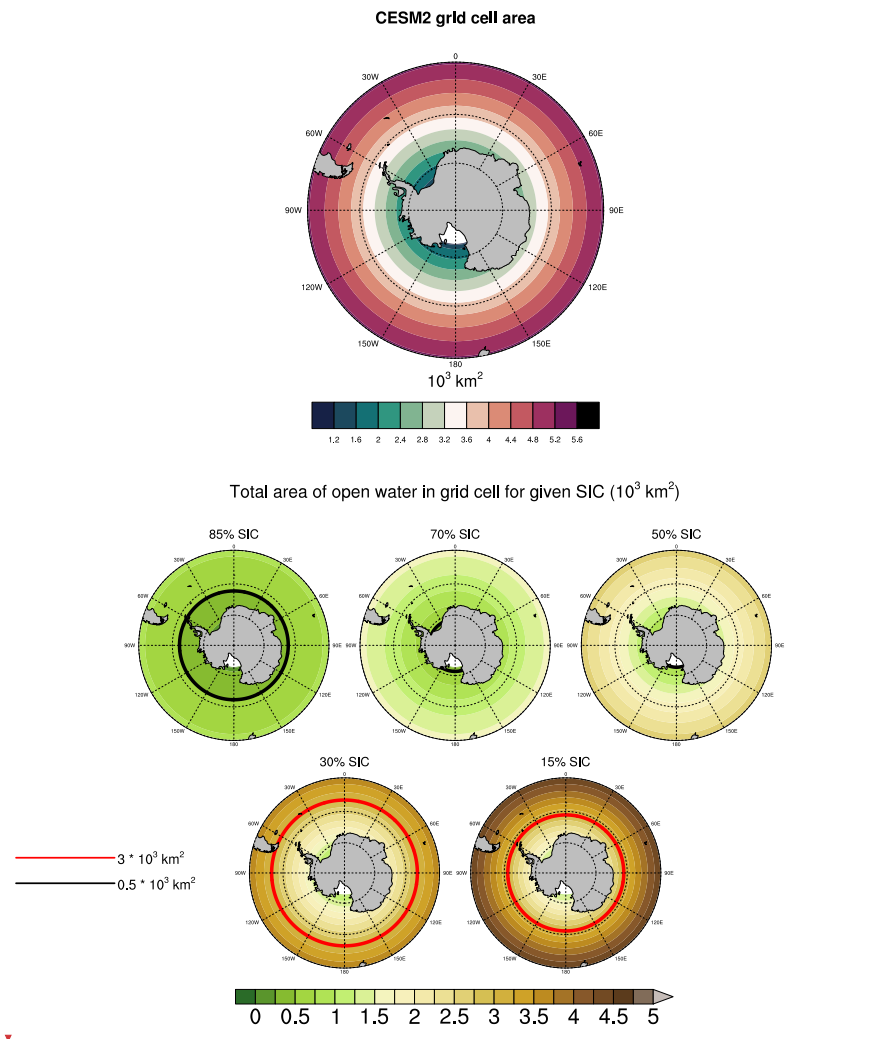
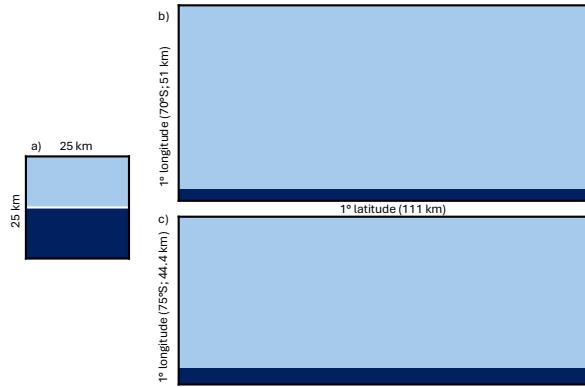


Figure B1. Area of the ocean grid cells in the CESM2 ($\times 10^3 \text{ km}^2$; top) and total area ($\times 10^3 \text{ km}^2$) of open water for a given SIC threshold in the CESM2 grid (bottom). Red/black contours indicate $3 \times 10^3 \text{ km}^2$ / $0.5 \times 10^3 \text{ km}^2$ of open water, respectively.



1705

Figure B2. Sea ice concentration required to result in 312.5 km² of open water within a grid cell: a) SIC 50% on a 25 km x 25 km equal area grid cell, b) 92% SIC on a 1°x1° lat/lon grid cell at 70°S (approximately 111km x 51km), and c) 84.4% SIC on a 1°x1° lat/lon grid cell at 75°S (approximately 111km x 44.4km)

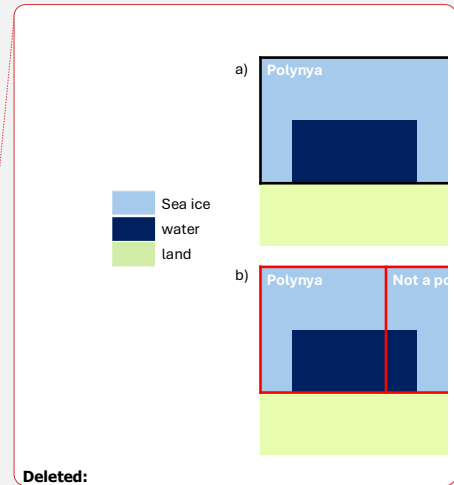
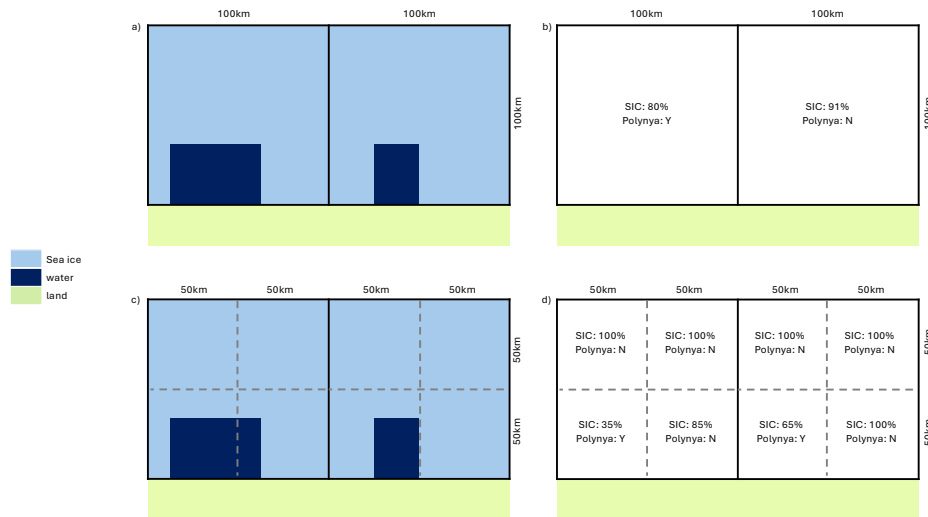


Figure B3. Examples of grid cells classified as polynyas using an 80% SIC threshold on a larger resolution grid (a-b) and a smaller resolution grid (c-d). Colored panels (a,c) indicate areas of ice (light blue), water (navy) and land (light green). Text in panels b,d indicate SIC for the grid cell and whether or not it would be identified as a polynya using an 80% SIC threshold. The top example has one polynya grid cell and double the integrated polynya area (10000 km²) over the entire region compared to the second example (2 grid cells and 5000 km²).

Appendix C: Degrading climate model daily SIC data.

Figure AC1 shows an example of model SICs that are degraded such that the new sea ice concentrations are set to 0 where the original SICs are less than 10% and also where SITs are less than 5 cm. In regions of SITs that fall between 5cm and 20 cm, SICs are set to half of the original values. The resulting degraded product has noticeably lower SICs along the ice perimeter and isolated locations near the Antarctic continent with lower SICs.

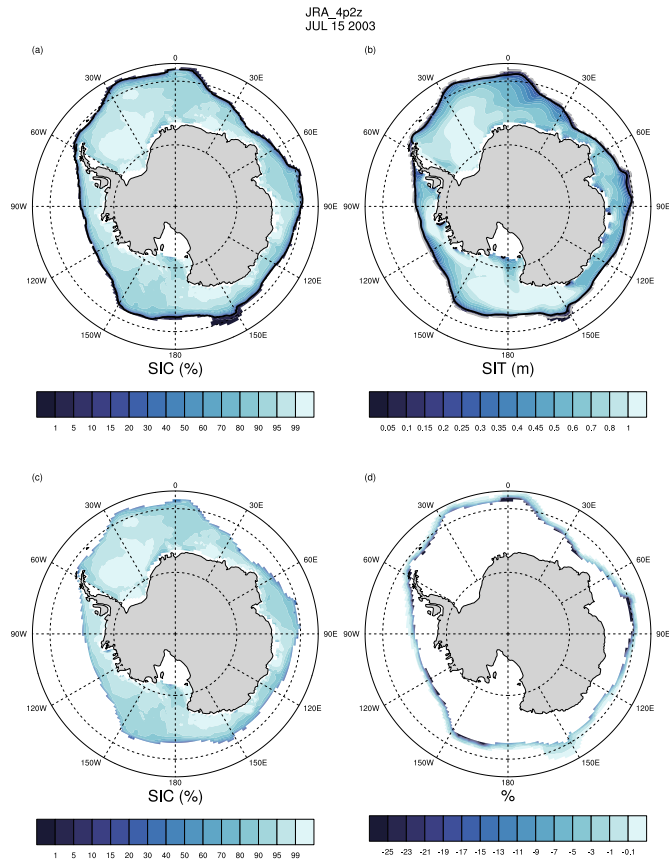


Figure C1. Sea Ice Concentration (a) and sea ice thickness (b) from the JRA-CESM run on July 15, 2003. Degraded sea ice (c) and (d) the resulting change in SIC by degrading the sea ice.

1730 Code and data availability

The CESM2-LE data used in this study are freely available, as described in Rodgers et al. (2021). The CESM2-LE and the JRA hindcast simulations (Forced Ocean Sea Ice, FOSI) are freely available from the Earth System Grid

(<https://www.earthsystemgrid.org/project/CESM.html>). The computational notebooks and other data processing tools used for this publication are freely available online (L.Landrum, 2024). Code for processing the data and making the figures will be published on a GitHub repository in final stages if paper is accepted for publication.

Author contributions

Study design and analysis were conducted by LL with ideas from MMH, AKD, KK and ZS. All authors contributed to the writing of the manuscript.

Competing Interests

1740 The authors declare that they have no conflict of interest.

Acknowledgements

The National Science Foundation (NSF) National Center for Atmospheric Research (NCAR) is sponsored by NSF under cooperative agreement no. 1852977. Previous and current CESM versions are freely available online (at <https://www.cesm.ucar.edu/models/cesm2/>). The CESM data sets used in this study are freely available online from the NCAR

1745 Digital Asset Services Hub (at <https://doi.org/10.5065/bgt9-tz46>). We thank all the scientists, software engineers, and administrators who contributed to the development and availability of CESM. The CESM project has been supported primarily by the National Science Foundation. We would like to acknowledge high-performance computing support from the Derecho system ([doi:10.5065/qx9a-pg09](https://doi.org/10.5065/qx9a-pg09)) provided by the Computational and Information Systems Laboratory at NSF NCAR.

1750 We acknowledge support for this work from National Aeronautics and Space Administration (NASA) and the National Science Foundation (NSF) as detailed below. Any opinions, findings, and conclusions or recommendations expressed in this material are those of the authors and do not necessarily reflect the views of these agencies. LL, MMH and KK acknowledge support for this work from the NASA Award 80NSSC20K1289 and the NSF Award 2037531. LL, AKD, KK and ZS acknowledge support for this work from the NASA Award 80NSSC21K1132.

1755

This study has been conducted using OSI SAF Global sea ice concentration climate data record 1978-2020 (v3.0, 2022), OSI-450-a, [doi:10.15770/EUM_SAF_OSI_0013](https://doi.org/10.15770/EUM_SAF_OSI_0013). EUMETSAT Ocean and Sea Ice Satellite Application Facility. Data extracted from E. U. Copernicus Marine Service Information: accessed 23 January, 2025.

References

- 1760 Arrigo, K. R., and G. L. van Dijken: Phytoplankton dynamics within 37 Antarctic coastal polynyas, *J. Geophys. Res.*, 108(C8), 3271, doi:[10.1029/2002JC001739](https://doi.org/10.1029/2002JC001739), 2003.
- [Arrigo, K. R., G. L. van Dijken, and A. L. Strong: Environmental controls of marine productivity hot spots around Antarctica, *J. Geophys. Res. Oceans*, 120, 5545–5565, doi:10.1002/2015JC010888, 2015.](#)
- [Comiso, J. C.: Characteristics of arctic winter sea ice from satellite multispectral microwave observations, *J. Geophys. Res.*, 91, 975–994, 1986.](#)
- 1765 [Bocquet, M., S. Fleury, F. Rémy, and F. Piras, F.: Arctic and Antarctic sea ice thickness and volume changes from observations between 1994 and 2023. *Journal of Geophysical Research: Oceans*, 129, e2023JC020848. <https://doi.org/10.1029/2023JC020848>, 2024.](#)
- [Cavalieri, D. J., P. Gloersen, and W. J. Campbell: Determination of sea ice parameters with the NIMBUS 7 SMMR, *J. Geophys. Res.*, 89, 5355–5369, 1984.](#)
- 1770 Comiso, J. C., [D. Cavalieri](#), [C. Parkinson](#) C., and [P. Gloersen](#): Passive microwave algorithms for sea ice concentrations: a comparison of two techniques. *Remote Sensing of the Environment*, 60, 357–384, 1997.
- [Crisciello, A. S., S. B. Das, M. J. Evans, K. E. Frey, H. Conway, I. Joughin, B. Medley, and E. J. Steig: Ice sheet record of recent sea-ice behavior and polynya variability in the Amundsen Sea, West Antarctica, *J. Geophys. Res. Oceans*, 118, 118–130, doi:10.1029/2012JC008077, 2013.](#)
- 1775 Danabasoglu, G., J. F. Lamarque, J. Baumeister, D. Bailey, A. K. DuVivier, J. Edwards, et al.: The Community Earth System Model version 2 (CESM2). *J. Adv. in Model. Earth Sys.*, 2, 1–35. <https://doi.org/10.1029/2019ms001916>, 2020.
- Duffy, G. A., F. Montiel, A. Purich, and C. I. Fraser: Emerging long-term trends and interdecadal cycles in Antarctic polynyas, *Proc. of the Nat. Acad. of Sc.*, 121 (11), <https://doi.org/10.1073/pnas.2321595121>, 2024.
- 1780 Diamond, R., L. C. Sime, C. R. Holmes, and D. Schroeder: CMIP6 models rarely simulate Antarctic winter sea-ice anomalies as large as observed in 2023. *Geophysical Research Letters*, 51(10), e2024GL109265. <https://doi.org/10.1029/2024GL109265>, 2024.
- DuVivier, A. K., M. M. Holland, L. Landrum, H. A. Singh, D. A. Bailey, and E. A. Maroon: Impacts of sea ice mushy thermodynamics in the Antarctic on the coupled Earth system, *Geophys. Res. Lett.*, 48, e2021GL094287, <https://doi.org/10.1029/2021GL094287>, 2021.
- 1785 [DuVivier, A. K., M. J. Molina, A. L. Deppenmeier, M. M. Holland, L. Landrum, K. Krumhardt, & S. Jenouvrier. Projections of winter polynyas and their biophysical impacts in the Ross Sea Antarctica. *Clim Dyn.* 2024;62\(2\):989-1012. doi:10.1007/s00382-023-06951-z. Epub 2023 Sep 23. PMID: 39328888; PMCID: PMC11424701, 2024.](#)
- Eyring, V., S. Bony, G. A. Meehl, C. A. Senior, B. Stevens, R. J. Stouffer, and K. E. Taylor: Overview of the Coupled Model
- 1790 Intercomparison Project Phase 6 (CMIP6) experimental design and organization. *Geosc. Model Devel.*, 9(5), 1937–1958, <https://doi.org/10.5194/gmd-9-1937-2016>, 2016.

- Fetterer, F., K. Knowles, W. N. Meier, M. Savoie, and A. K. Windnagel: Sea Ice Index, Version 3. Distributed by National Snow and Ice Data Center, Boulder, Colorado, USA (accessed 2 June 2023); <https://doi.org/10.7265/NSK072F8>, 2017.
- 1795 Flores, H., G. Veyssière, G. Castellani, *et al.*: Sea-ice decline could keep zooplankton deeper for longer. *Nat. Clim. Chang.* 13, 1122–1130, <https://doi.org/10.1038/s41558-023-01779-1>, 2023.
- Fogt, R. L., A. M. Sleinkofer, M. N. Raphael, *et al.*: A regime shift in seasonal total Antarctic sea ice extent in the twentieth century. *Nat. Clim. Chang.* 12, 54–62, <https://doi.org/10.1038/s41558-021-01254-9>, 2022.
- [Fons, S., Kurtz, N., and Bagnardi, M.: A decade-plus of Antarctic sea ice thickness and volume estimates from CryoSat-2 using a physical model and waveform fitting, *The Cryosphere*, 17, 2487–2508, https://doi.org/10.5194/tc-17-2487-2023, 2023.](https://doi.org/10.5194/tc-17-2487-2023)
- 1800 [Fraser, A. D. K. I. Ohshima, S. Nihashi, R. A. Massom, T. Tamura, K. Nakata, G. D. Williams, S. Carpentier, and S. Willmes: Landfast ice controls on sea-ice production in the Cape Darnley Polynya: A case study, *Remote Sensing of Environment*, Volume 233, 111315, ISSN 0034-4257, https://doi.org/10.1016/j.rse.2019.111315, 2019.](https://doi.org/10.1016/j.rse.2019.111315)
- Gilbert, R. O.: *Statistical Methods for Environmental Pollution Monitoring*, Wiley, NY, 1987.
- Harrison, T. C., S. Biri, T. J. Bracegirdle, J. C. King, E. C. Kent, E. Vignon, and J. Turner, J.: Reanalysis representation of low-level winds in the Antarctic near-coastal region, *Weather Clim. Dynam.*, 3, 1415–1437, <https://doi.org/10.5194/wcd-3-1415-2022>, 2022.
- 1805 Grenfell, T. C., D. J. Cavalieri, J. C. Comiso, M. R. Drinkwater, R. G. Onstott, I. Rubinstein, K. Steffen, and D. P. Winebrenner: Considerations for microwave remote sensing of thin sea ice, in: *Microwave Remote Sensing of Sea Ice*, edited by: Carsey, F. D., American Geophysical Union, Washington, D.C., doi:10.1029/GM068p0291, 1992.
- 1810 Holmes, C. R., T. J. Bracegirdle, P. R. Holland, J. Stroeve, and J. Wilkinson: Brief communication: New perspectives on the skill of modelled sea ice trends in light of recent Antarctic sea ice loss, *The Cryosphere*, 18, 5641–5652, <https://doi.org/10.5194/tc-18-5641-2024>, 2024.
- Hobbs, W., and Coauthors: Observational Evidence for a Regime Shift in Summer Antarctic Sea Ice. *J. Climate*, 37, 2263–2275, <https://doi.org/10.1175/JCLI-D-23-0479.1>, 2024.
- 1815 [Holland, M. M., C. M. Bitz, E. C. Hunke, W. H. Lipscomb, and J. L. Schramm: Influence of the sea ice thickness distribution on polar climate in CCSM3. *Journal of Climate*, 19\(11\), 2398–2414. https://doi.org/10.1175/jcli3751.1, 2006.](https://doi.org/10.1175/jcli3751.1)
- Hunke, E. C., W. H. Lipscomb, A. K. Turner, N. Jeffery, and S. Elliott: CICE: The Los Alamos Sea Ice Model. Documentation and software user's manual. Version 5.1. T-3 Fluid Dynamics Group, Los Alamos National Laboratory, Tech. Rep. LA-CC-06-012, 2015.
- 1820 Ivanova, N., L. T. Pedersen, R. T. Tonboe, S. Kern, G. Heygster, T. Lavergne, A. Sorensen, R., Saldo, G. Dybjakaer, L. Brucker, and M. Shokr: Inter-comparison and evaluation of sea ice algorithms: towards further identification of challenges and optimal approach using passive microwave observations, *The Cryo.*, 9, 1797–1817, <https://doi.org/10.5194/tc-9-1797-2015>, 2015.
- [Jeong, H., S. S. Lee, H. S. Park, *et al.*: Future changes in Antarctic coastal polynyas and bottom water formation simulated by a high-resolution coupled model. *Commun Earth Environ* 4, 490. https://doi.org/10.1038/s43247-023-01156-y, 2023.](https://doi.org/10.1038/s43247-023-01156-y)

- 1825 Jones, R., I. Renfrew, A. Orr, B. Webber, D. Holland, and M. Lazzara: Evaluation of four global reanalysis products using in situ observations in the Amundsen Sea Embayment, Antarctica, *J. Geophys. Res.-Atmos.*, 121, 6240–6257, 2016.
- Kacimi, S., and R. Kwok: Arctic snow depth, ice thickness, and volume from ICESat-2 and CryoSat-2: 2018–2021. *Geophys. Res. Letts.*, 49, e2021GL097448. <https://doi.org/10.1029/2021GL097448>, 2022.
- Kendall, M.G.: Rank Correlation Methods, 4th edition, Charles Griffin, London, 1975.
- 1830 Kern, S., G. Spreen, L. Kaleschke, S. De La Rosa, and G. Heygster: Polynya Signature Simulation Method polynya area in comparison to AMSR-E 89GHz sea-ice concentrations in the Ross Sea and off the Adélie Coast, Antarctica, for 2002–05: first results, *Ann. Glaciol.*, 46, 409–418, 2007.
- Kobayashi ,S., O. T. A. Yukinari, Y. Harada, A. Ebita, M. Moriya, H. Onoda, K. Onogi, H. Kamahori, C. Kobayashi, K. Miyaoka, and K. Takahahi: The JRA-55 reanalysis: general specifications and basic characteristics. *J Meteorol Soc Jpn Ser II* 93(1), 5–48, <https://doi.org/10.2151/jmsj.2015-001>, 2015.
- 1835 Krumhardt K. M., M. C. Long, A. T. Sylvester, and C. M. Petrik: Climate drivers of Southern Ocean phytoplankton community composition and potential impacts on higher trophic levels. *Front. Mar. Sci.* 9:916140. doi: 10.3389/fmars.2022.916140, 2022.
- Krumhardt, K. M., M. C. Long, C. M. Petrik, M. Levy, F. S. Castruccio, K. Lindsay, L. Romashkov, A.-L. Deppenmeier, R. Denéchére, Z. Chen, L. Landrum, G. Danabasoglu, and P. Chang: From nutrients to fish: Impacts of mesoscale processes in a global CESM-FEISTY eddying ocean model framework, *Prog. in Ocean.*, 227, 2024, 103314, ISSN 0079-6611, <https://doi.org/10.1016/j.pocean.2024.103314>, 2024.
- 1840 Kwok, R., J. C. Comiso, S. Martin, and R. Drucker: Ross Sea polynyas: Response of ice concentration retrievals to large areas of thin ice, *J. Geophys. Res.*, 112, C12012, doi:10.1029/2006JC003967, 2007.
- Labrousse, S., A. D. Fraser, M. Sumner, T. Tamura, D. Pinaud, B. Wienecke, et al.: Dynamic fine-scale sea icescape shapes adult emperor penguin foraging habitat in East Antarctica. *Geophys. Res. Lett.* 46, 11206–11218. doi: 10.1029/2019GL084347, 2019.
- Lavergne, T., A. M. Sørensen, S. Kern, R. Tonboe, D. Notz, S. Aaboe, L. Bell, G. Dybkjær, S. Eastwood, C. Gabarro, G. Heygster, M. A. Killie, M. Brandt Kreiner, J. Lavelle, R. Saldo, S. Sandven, and L. T. Pedersen: Version 2 of the EUMETSAT OSI SAF and ESA CCI sea-ice concentration climate data records, *The Cryo.*, 13, 49–78, [https://doi.org/10.5194/tc-13-49-](https://doi.org/10.5194/tc-13-49-2019)
- 1850 2019, 2019.
- Li, Y., R. Ji, S. Jenouvrier, M. Jin, and J. Stroeve: Synchronicity between ice retreat and phytoplankton bloom in circum-Antarctic polynyas, *Geophys. Res. Lett.*, 43, 2086–2093, doi:10.1002/2016GL067937, 2016.
- Mann, H.B.: Non-parametric tests against trend, *Econometrica* 13:163-171, 2045.
- Markus, T. and B. A. Burns: Detection of coastal polynyas with passive microwave data. *Ann. Glaciol.*, 17, 351- 355, 1993.
- 1855 Massom, R. A., P. T. Harris, K. J. Michael, and M. J. Potter: The distribution and formative processes of latent-heat polynyas in East Antarctica, *Ann. Glaciol.*, 27, 420– 426, 1998.
- Meier, W.N.: Comparison of passive microwave ice concentration algorithm retrievals with AVHRR imagery in Arctic peripheral seas. *IEEE Trans. Geo. Remote Sensing*, 43, 1324-1337, 2005.

- Meier, W. N., G. Peng, D. J. Scott, and M. H. Savoie: Verification of a new NOAA/NSIDC passive microwave sea-ice concentration climate record. *Polar Research*, 33. doi: 10.3402/polar.v33.21004, 2014.
- 1860 Meier, W. N., F. Fetterer, A. K. Windnagel, and J. S. Stewart: *NOAA/NSIDC Climate Data Record of Passive Microwave Sea Ice Concentration, Version 4*. Southern Hemisphere, 1979–2020. Boulder, Colorado USA. NSIDC: National Snow and Ice Data Center. doi: <https://doi.org/10.7265/efmz-2t65>, 2021. Accessed June 3, 2023.
- Meier, W. N., A. Windnagel, and S. Stewart: CDR Climate Algorithm and Theoretical Basis Document: Sea Ice Concentration.
- 1865 NOAA NCEI CDR Program, 2021.
- Mohrmann, M., C. Heuzé, and S. Swart: Southern Ocean polynyas in CMIP6 models, *The Cryo.*, 15, 4281–4313, <https://doi.org/10.5194/tc-15-4281-2021>, 2021.
- Nakata, K., K. I. Ohshima, S. Nihashi, N. Kimura, and T. Tamura: Variability and ice production budget in the Ross Ice Shelf Polynya based on a simplified polynya model and satellite observations, *J. of Geophys. Res.: Oceans*, 120, 6234–6252, 2015.
- 1870 Nakata, K., K. I. Ohshima, and S. Nihashi: Mapping of Active Frazil for Antarctic Coastal Polynyas, With an Estimation of Sea-Ice Production. *Geophys. Res. Lett.*, 48, e2020GL091353, 2021.
- Nihashi, S. and K. J. Ohshima: Circumpolar Mapping of Antarctic Coastal Polynyas and Landfast Sea Ice: Relationship and Variability, *J. Clim.*, 28, 3650–3670, DOI: 10.1175/JCLI-D-14-00369.1, 2015.
- Notz, D.: Sea-ice extent and its trend provide limited metrics of model performance.
- 1875 *Cryo.* 8, 229–243. (doi:10.5194/tc-8-229-2014), 2014.
- Notz, D.: How well must climate models agree with observations?, *Philosophical Transactions of the Royal Society of London A: Mathematical, Phys. and Engin. Sci.*, 373, <https://doi.org/10.1098/rsta.2014.0164>, 2015.
- [Oliver, H., J. S. Turner, A. Castagna, H. Houskeeper, and H. Dierssen: High Antarctic coastal productivity in polynyas revealed by considering remote sensing ice-adjacency effects. *Limnol. Oceanogr. Lett.* <https://doi.org/10.1002/lol2.70043>, 2025.](#)
- 1880 [Ohshima, K., Y. Fukamachi, G. Williams, et al.: Antarctic Bottom Water production by intense sea-ice formation in the Cape Darnley polynya. *Nature Geosci* 6, 235–240. <https://doi.org/10.1038/ngeo1738>, 2013.](#)
- Ohshima, K. I., S. Nihashi, and K. Iwamoto, K.: Global view of sea-ice production in polynyas and its linkage to dense/bottom water formation, *Geoscience Letters*, 3, 13, 2016.
- O'Reilly, J. E., S. Maritorena, B. G. Mitchell, D. A. Siegel, K. L. Carder, S. A. Garver, M. Kahru, and C. McClain, C.: Ocean color chlorophyll algorithms for SeaWiFS, *J. Geophys. Res.*, 103, 24,937– 24,953, 1998.
- 1885 OSI SAF Global sea ice concentration climate data record 1978–2020 (v3.0, 2022), OSI-450-a, doi:10.15770/EUM_SAF_OSI_0013. EUMETSAT Ocean and Sea Ice Satellite Application Facility. Data extracted from E. U. Copernicus Marine Service Information: accessed 23 January, 2025.
- Parkinson, C. L. and D. J. Cavalieri: Antarctic sea ice variability and trends, 1979–2010, *The Cryo.*, 6, 871–880, <https://doi.org/10.5194/tc-6-871-2012>, 2012.
- 1890 Parkinson, C., and D. Cavalieri: Antarctic sea ice variability and trends, 1979–2010. *The Cryosphere*, 6, 871–880, 2012.

- Parkinson, C. L.: A 40-y record reveals gradual Antarctic sea ice increases followed by decreases at rates far exceeding the rates seen in the Arctic, *P. Natl. Acad. Sci. USA*, 116, 14414–14423, 2019.
- Purich, A., and E. W. Doddridge: Record low Antarctic sea ice coverage indicates a new sea ice state. *Commun Earth Environ* 4, 314. <https://doi.org/10.1038/s43247-023-00961-9>, 2023.
- Raphael, M.N., and M. S. Hancock: A new record minimum for Antarctic sea ice. *Nat Rev Earth Environ* 3, 215–216. <https://doi.org/10.1038/s43017-022-00281-0>, 2022.
- Richert, I., P. Yager, J. Dinasquet, R., Logares, L. Riemann, A. Wendeberg, S. Bertilsson, and D. Scofield: Summer comes to the Southern Ocean: how phytoplankton shape bacterioplankton communities far into the deep dark sea. *Ecosphere*. 10. e02641. 10.1002/ecs2.2641, 2019.
- Raphael, M. N., T. J. Maierhofer, R. L. Fogt, W. R. Hobbs, and M. S. Hancock: A Twenty-First Century Structural Change in Antarctica's Sea Ice System. *Communications Earth & Environment* 6, no. 1 (February 21, 2025): 1–9. <https://doi.org/10.1038/s43247-025-02107-5>, 2025
- Roach, L. A., J. Dörr, C. R. Holmes, F. Massonnet, E. W. Blockley, D. Notz, et al.: Antarctic sea ice area in CMIP6. *Geophysical Research Letters*, 47, e2019GL086729. <https://doi.org/10.1029/2019GL086729>, 2020.
- Singh, H. K. A., L. Landrum, M. M. Holland, D. A. Bailey, and A. K. DuVivier: An overview of Antarctic sea ice in the CESM2: analysis of the seasonal cycle, predictability, and atmosphere-ocean-ice interactions. *J Adv Model Earth Syst.*, 13, <https://doi.org/10.1029/2020MS002143>, 2020.
- Smith, A., A. Jahn, and M. Wang, M.: Seasonal transition dates can reveal biases in Arctic sea ice simulations, *The Cryosphere*, 14, 2977–2997, <https://doi.org/10.5194/tc-14-2977-2020>, 2020.
- Smith, A., Jahn, A., Burgard, C., and Notz, D.: Improving model-satellite comparisons of sea ice melt onset with a satellite simulator, *The Cryosphere*, 16, 3235–3248, <https://doi.org/10.5194/tc-16-3235-2022>, 2022.
- Stammerjohn, S. E., D. G. Martinson, R. C. Smith, X. Yuan, and D. Rind: Trends in Antarctic annual sea ice retreat and advance and their relation to El Niño–Southern Oscillation and Southern Annular Mode variability, *J. Geophys. Res.*, 113, C03S90, doi:10.1029/2007JC004269, 2008.
- Tamura, T., K. I. Ohshima, H. Enomoto, K. Tateyama, A. Muto, S. Ushio, and R. A. Massom: Estimation of thin sea-ice thickness from NOAA AVHRR data in a polynya off the Wilkes Land coast, East Antarctica. *Ann. Glaciol.*, 44, 269–274, 2006.
- Tamura, T., K. I. Ohshima, T. Markus, D. J. Cavalieri, S. Nishashi, and N. Hirasawa: Estimation of thin ice thickness and detection of fast ice from SSM/I data in the Antarctic Ocean, *J. Atmos. Oceanic Technol.*, 24, 1757– 1772, 2007.
- Tamura, T., K. I. Ohshima, and S. Nishashi: Mapping of sea ice production for Antarctic coastal polynyas. *Geophys Res Lett* 35:L07606, 2008.
- Tamura, T., K. I. Ohshima, A. D. Fraser, and G. D. Williams: Sea ice production variability in Antarctic coastal polynyas, *J. Geophys. Res. Oceans*, 121, 2967–2979, doi:10.1002/2015JC011537, 2016.

Deleted: Rodgers, K. B., Lee, S.-S., Rosenbloom, N., Timmermann, A., Danabasoglu, G., Deser, C., Edwards, J., Kim, J.-E., Simpson, I. R., Stein, K., Stuecker, M. F., Yamaguchi, R., Bóday, T., Chung, E.-S., Huang, L., Kim, W. M., Lamarque, J.-F., Lombardozzi, D. L., Wiedner, W. R., and Yeager, S. G.: Ubiquity of human-induced changes in climate variability, *Earth Syst. Dynam.*, 12, 1393–1411, <https://doi.org/10.5194/esd-12-1393-2021>, 2021.*

- Thompson, L., M. Smith, J. Thomson, S. Stammerjohn, S. Ackley, and B. Loose: Frazil ice growth and production during katabatic wind events in the Ross Sea, Antarctica, *The Cryosphere*, 14, 3329–3347, <https://doi.org/10.5194/tc-14-3329-2020>, 2020.
- 1935 Tsujino, H., S. Urakawa, H. Nakano, R. J. Small, W. M. Kim, S. G. Yeager, G. Danabasoglu, T. Suzuki, J. L. Bamber, M. Bentsen, C. W. Böning, A. Bozec, E. P. Chassignet, E. Curchitser, F. Boeira Dias, P. J. Durack, S. M. Griffies, Y. Harada, M. Ilicak, S. A. Josey, C. Kobayashi, S. Kobayashi, Y. Komuro, W. G. Large, J. Le Sommer, S. J. Marsland, S. Masina, M. Scheinert, H. Tomita, M. Valdivieso, and D. Yamazaki: Jra-55 based surface dataset for driving ocean–sea-ice models (jra55-do). *Ocean Modelling*, **130**:79–139, 2018.
- 1940 Turner, J., T. Phillips, G. J. Marshall, J. S. Hosking, J. O. Pope, T. J. Bracegirdle, and P. Deb: Unprecedented springtime retreat of Antarctic sea ice in 2016, *Geophys. Res. Lett.*, 44, 6868–6875, 2017.
- Turner, J., C. Holmes, T. Caton Harrison, T. Phillips, B. Jena, T. Reeves-Francois, R. Fogt, E. R. Thomas, and C. C. Bajish: Record low Antarctic sea ice cover in February 2022. *Geophys. Res. Lett.*, 49, e2022GL098904, 2022.
- Windnagel, A., Meier, W., Stewart, S., Fetterer, F., & Stafford, T.: NOAA/NSIDC Climate Data Record of Passive Microwave Sea Ice Concentration Version 4 Analysis. NSIDC Special Report 20. Boulder CO, USA: National Snow and Ice Data Center, 2021.
- [World Meteorological Organization: WMO sea-ice nomenclature. Terminology, codes and illustrated glossary. Geneva, Secretariat of the World Meteorological Organization, 1970. \[ix\], 147 p. \[including 175 photos\] + corrigenda slip. \(WMO/OMM/BMO, No. 259, TP. 145.\). Edition 1970.](#)
- 1950 Zygmuntowska, M., P. Rampal, N. Ivanova, and L. H. Smedsrud: Uncertainties in Arctic sea ice thickness and volume: new estimates and implications for trends, *The Cryosphere*, 8 (2), 705–720, doi:10.5194/tc-8-705-2014, 2014.

▼
▲
Page 4: [1] Deleted **Laura Landrum** **8/27/25 1:53:00 PM**

▼
▲
Page 4: [2] Deleted **Laura Landrum** **8/27/25 11:48:00 AM**

▼
▲
Page 12: [3] Deleted **Laura Landrum** **9/3/25 5:23:00 PM**

▼
▲
Page 12: [3] Deleted **Laura Landrum** **9/3/25 5:23:00 PM**

▼
▲
Page 12: [3] Deleted **Laura Landrum** **9/3/25 5:23:00 PM**

▼
▲
Page 12: [3] Deleted **Laura Landrum** **9/3/25 5:23:00 PM**

▼
▲
Page 12: [3] Deleted **Laura Landrum** **9/3/25 5:23:00 PM**

▼
▲
Page 12: [3] Deleted **Laura Landrum** **9/3/25 5:23:00 PM**

▼
▲
Page 12: [3] Deleted **Laura Landrum** **9/3/25 5:23:00 PM**

▼
▲
Page 12: [4] Deleted **Laura Landrum** **9/3/25 5:25:00 PM**

▼
▲
Page 12: [4] Deleted **Laura Landrum** **9/3/25 5:25:00 PM**

▼
▲
Page 12: [4] Deleted **Laura Landrum** **9/3/25 5:25:00 PM**

▼
▲
Page 12: [4] Deleted **Laura Landrum** **9/3/25 5:25:00 PM**

▼
▲
Page 12: [4] Deleted **Laura Landrum** **9/3/25 5:25:00 PM**

▼
▲
Page 12: [4] Deleted **Laura Landrum** **9/3/25 5:25:00 PM**

▼
▲

▼
▲
Page 12: [4] Deleted **Laura Landrum** **9/3/25 5:25:00 PM**

▼
▲
Page 12: [4] Deleted **Laura Landrum** **9/3/25 5:25:00 PM**

▼
▲
Page 16: [5] Deleted **Laura Landrum** **9/4/25 2:43:00 PM**

▼
▲
Page 16: [6] Deleted **Laura Landrum** **9/4/25 3:40:00 PM**

▼
▲
Page 17: [7] Deleted **Laura Landrum** **9/4/25 3:45:00 PM**

▼
▲
Page 17: [8] Deleted **Laura Landrum** **9/4/25 3:23:00 PM**

▼
▲
Page 19: [9] Deleted **Laura Landrum** **9/5/25 11:02:00 AM**

▼
▲
Page 19: [10] Deleted **Laura Landrum** **9/5/25 10:53:00 AM**

▼
▲
Page 19: [11] Deleted **Laura Landrum** **9/5/25 12:41:00 PM**

▼
▲
Page 20: [12] Deleted **Laura Landrum** **9/5/25 4:12:00 PM**

▼
▲
Page 20: [13] Deleted **Laura Landrum** **9/5/25 4:17:00 PM**

▼
▲
Page 20: [14] Deleted **Laura Landrum** **9/6/25 4:23:00 PM**

▼
▲
Page 20: [15] Deleted **Laura Landrum** **9/6/25 4:27:00 PM**

▼
▲
Page 23: [16] Deleted **Laura Landrum** **9/4/25 3:47:00 PM**
x

